Resolving cool evolved stars:

From the photosphere to the dust formation zone

Context:
From 1^{st} to 2^{nd} generation VLTI instruments

From 1D to 3D atmosphere models

Markus Wittkowski (ESO),
based on different projects with several collaborators

Cool evolved stars

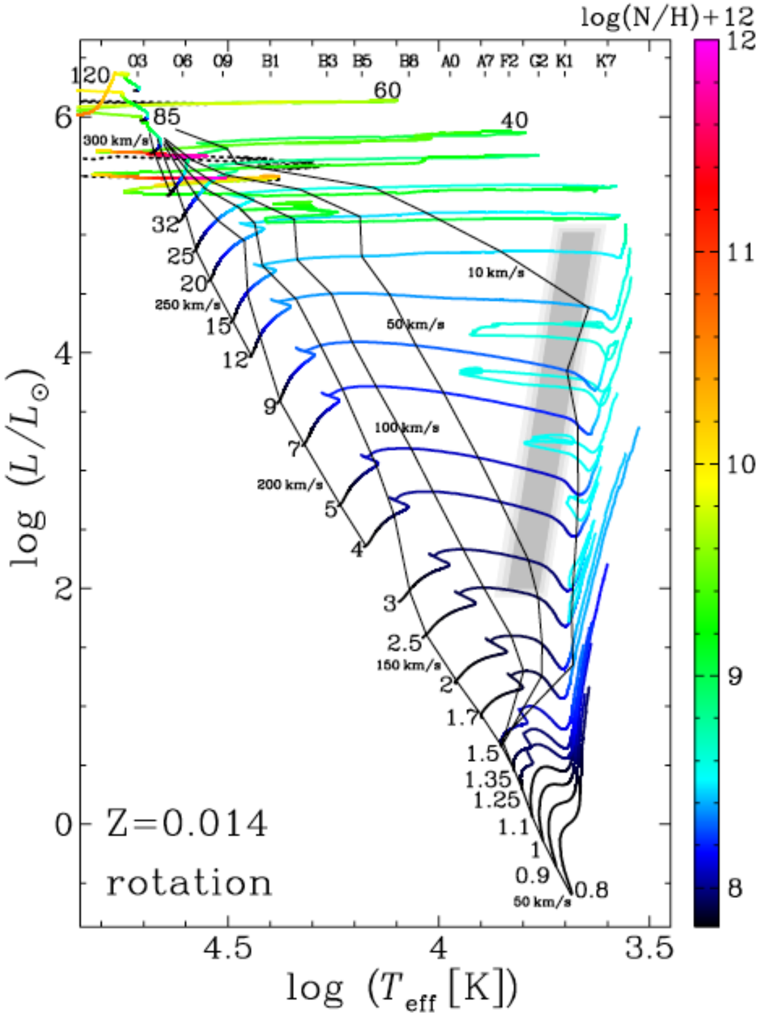

Evolutionary tracks with rotation from Ekström et al. (2012)

- Red giants, AGB stars (SR, Mira, OH/IR), red supergiants
- Along the Hayashi track in the HR diagram
- Low effective temperatures between about 2500K and 4000K and low surface gravities

Cool evolved stars: Pulsations

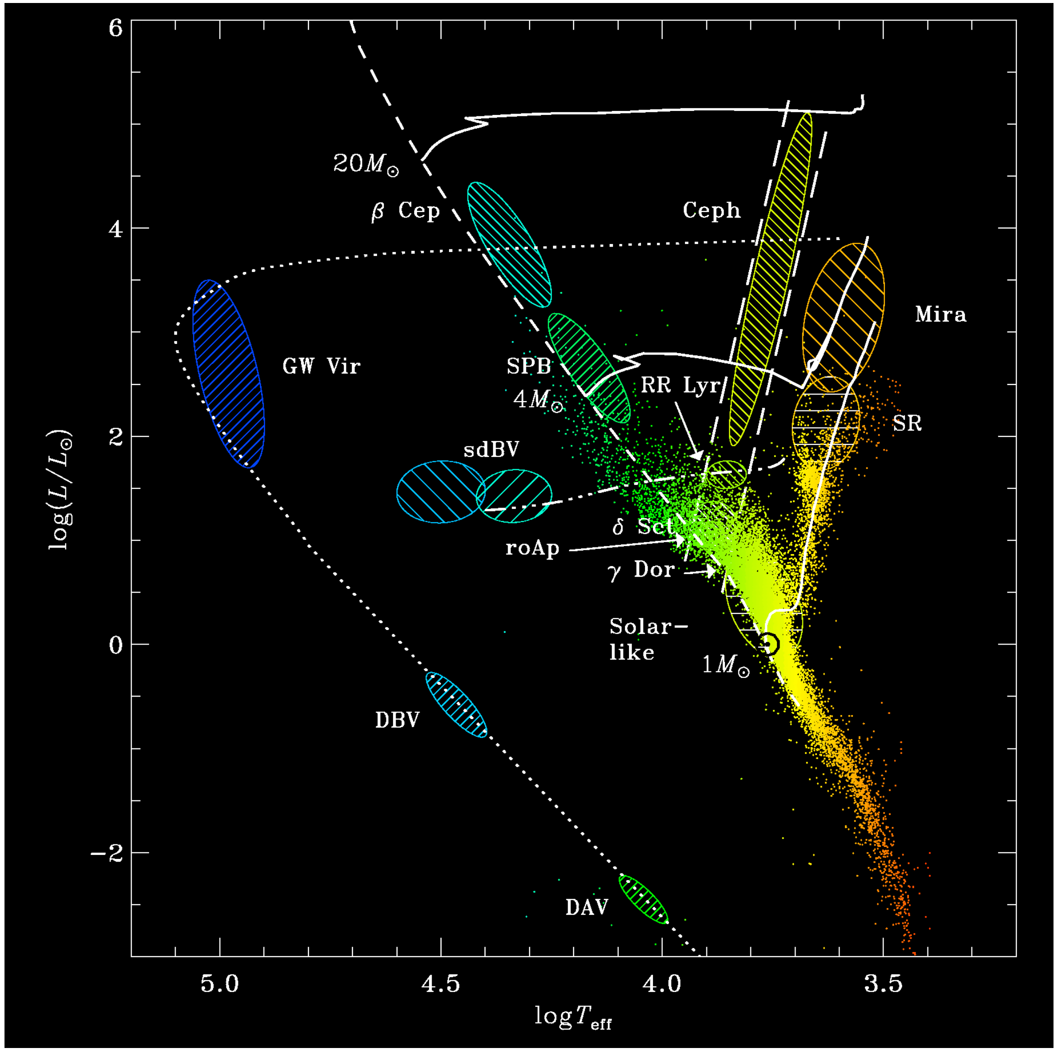

Fig. from Jørgen Christensen-Dalsgaard

- AGB stars are affected by pulsations with typical periods of the order of 1 yr and amplitudes of up to 0.5-1 mag (near-IR, bol.)
- Variable red supergiants have typical amplitudes of 0.25 mag, i.e. ~3 times less than AGB stars (e.g. Wood et al. 1983).

Cool evolved stars: Convection

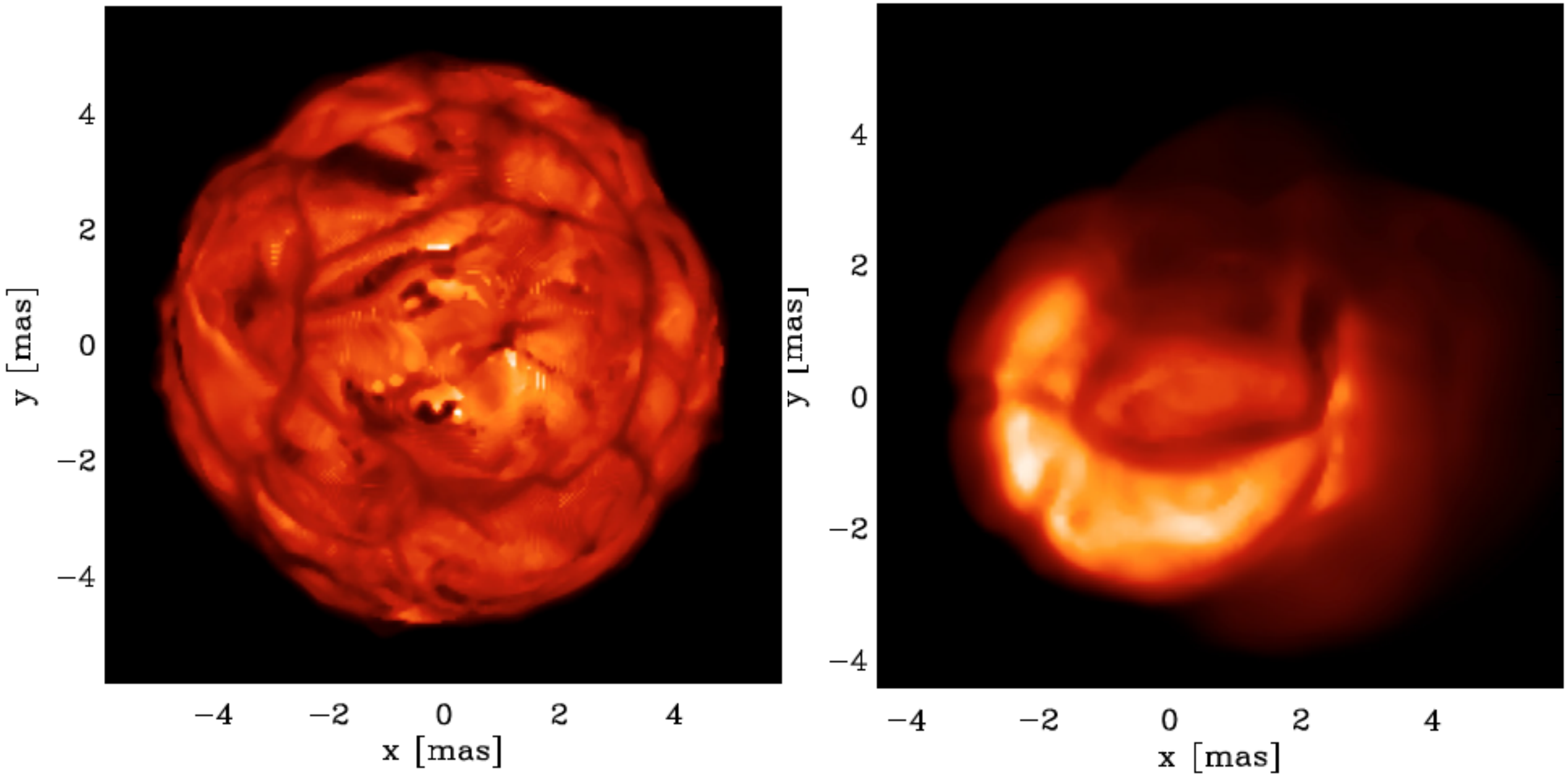

3D simulations at 1.6 μm of a RSG (left) and AGB (right) star from Chiavassa et al. (2010)

Cool evolved stars: Mass loss

- Measured mass-loss rates from CO (de Beck et al. 2010):
  - AGB stars: 4×10^{-8} M_{sun}/yr - 8×10^{-5} M_{sun}/yr
  - RSG stars: 2×10^{-7} M_{sun}/yr - 3×10^{-4} M_{sun}/yr
- Thought to be triggered by shocks induced by pulsation and convection that extend the atmospheres, dust formation, and radiative acceleration on dust grains dragging along the gas. Well constrained for carbon-rich Miras. Details are surprisingly little understood, in particular for oxygen rich Mira stars, and even less for semi-regular AGB stars, RSGs.
- Shaping processes toward PNe thought to be dominated by the effects of companions (de Marco 2009). Also, 70% of all massive stars will exchange mass with a companion (Sana+ 2012).
- Effects of companions, and of other shaping mechanism (convection, magnetic fields) on the inner atmospheric molecular layers, where the mass loss is initiated?

Structure of an AGB star

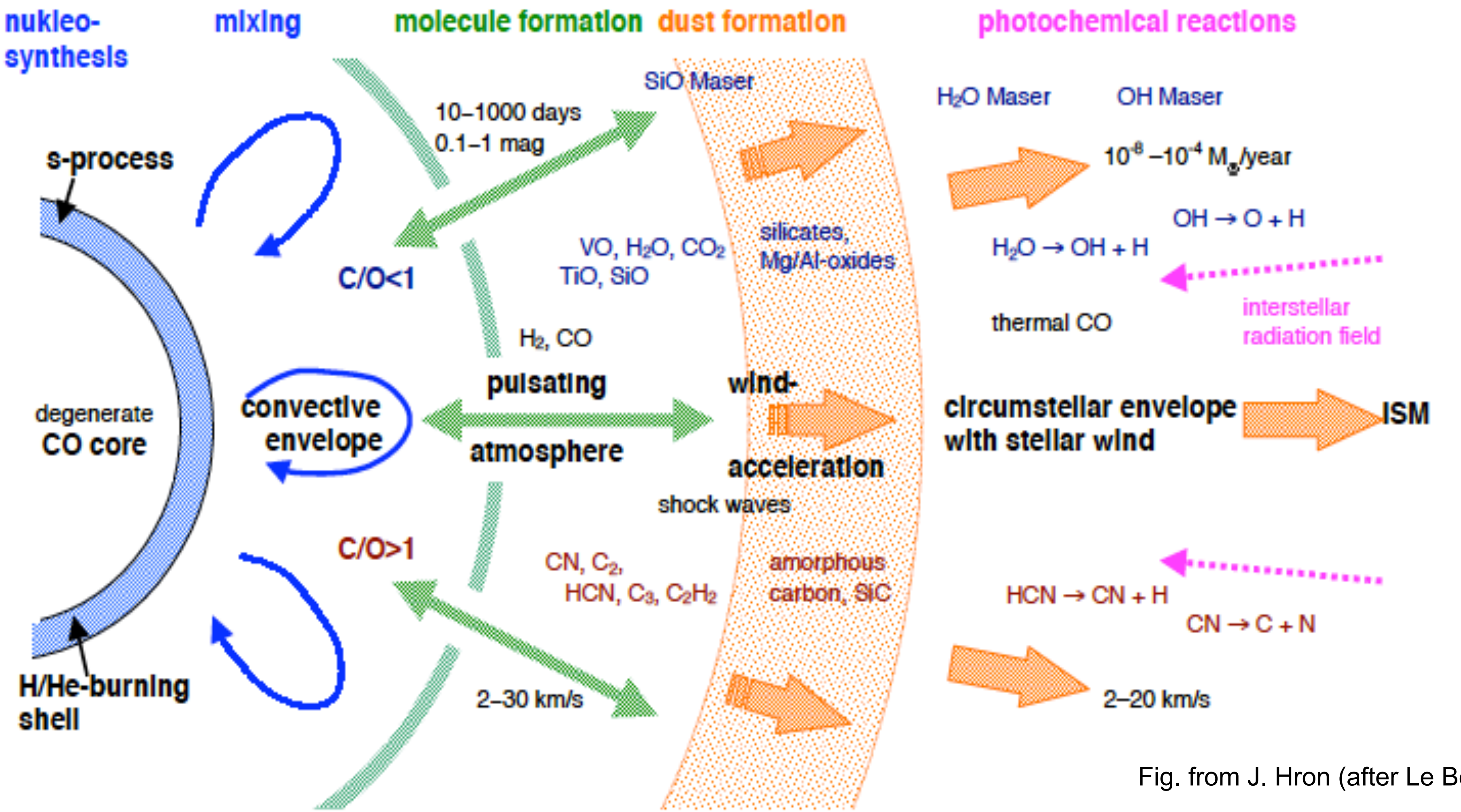

Fig. from J. Hron (after Le Bertre)

Structure of an AGB star

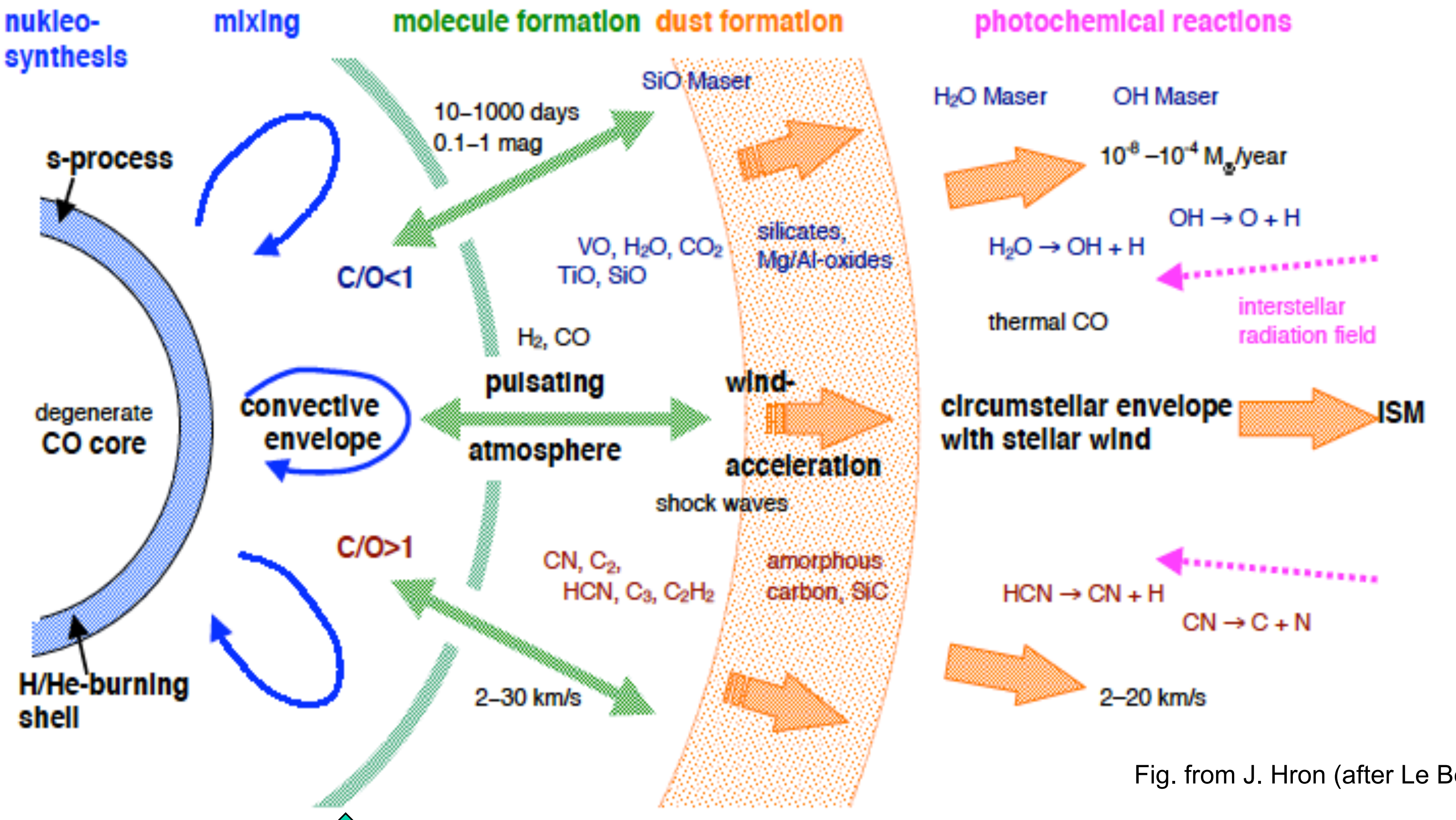

Fig. from J. Hron (after Le Bertre)

Photosphere (difficult to measure, difficult to define a “radius”)

Structure of an AGB star

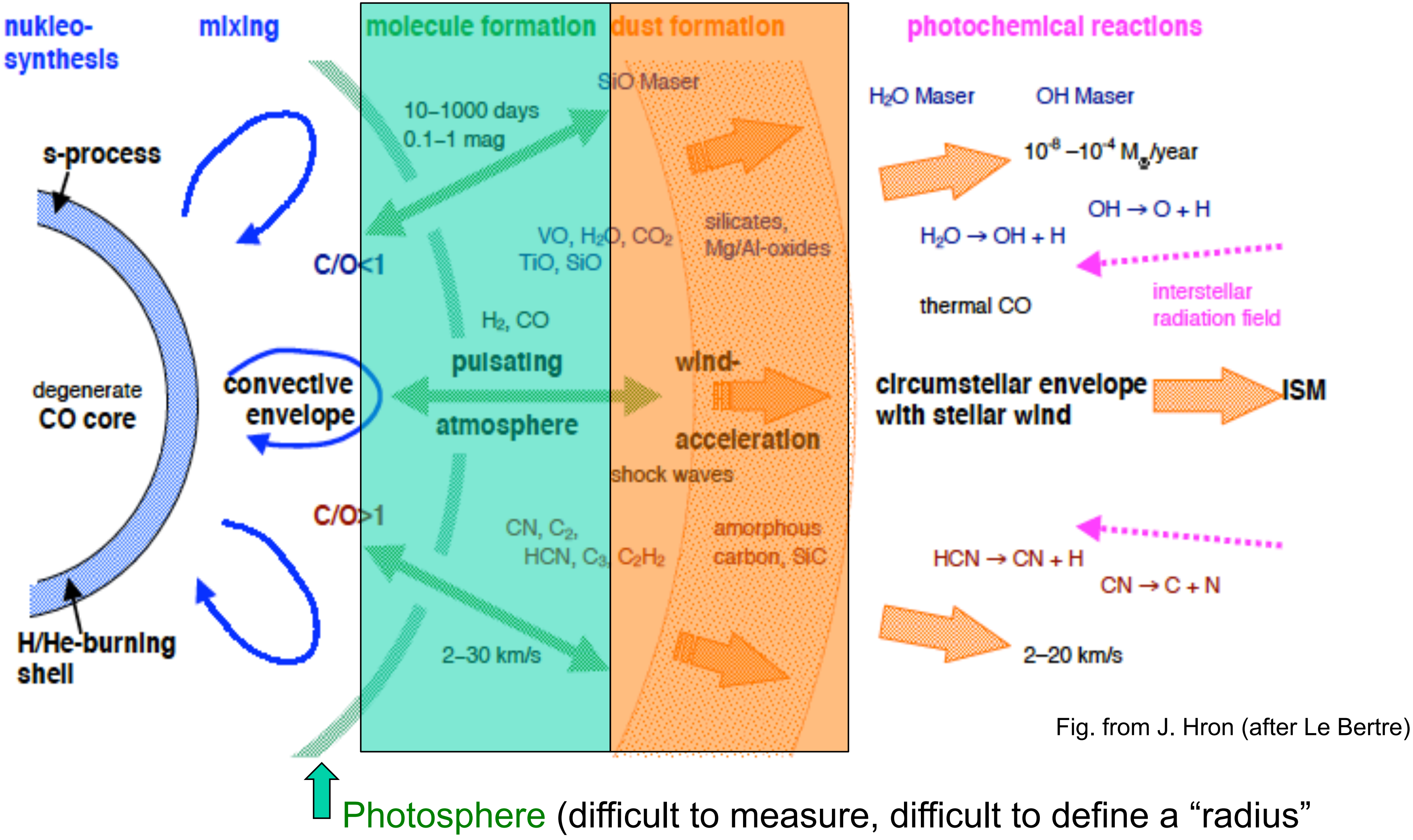

Fig. from J. Hron (after Le Bertre)

Photosphere (difficult to measure, difficult to define a “radius”

Cool evolved stars: Interferometry

- Direct measurement of angular diameters
- Direct measurement of the effective temperature based on the measured bolometric flux and the angular diameter
- Structure/stratification of the atmospheres
- Molecular layers
- Surface inhomogeneities
- Most of this requires spectral resolution to separate continuum and molecular layers -> spectro-interferometry

VLTI: A virtual 100-metre telescope

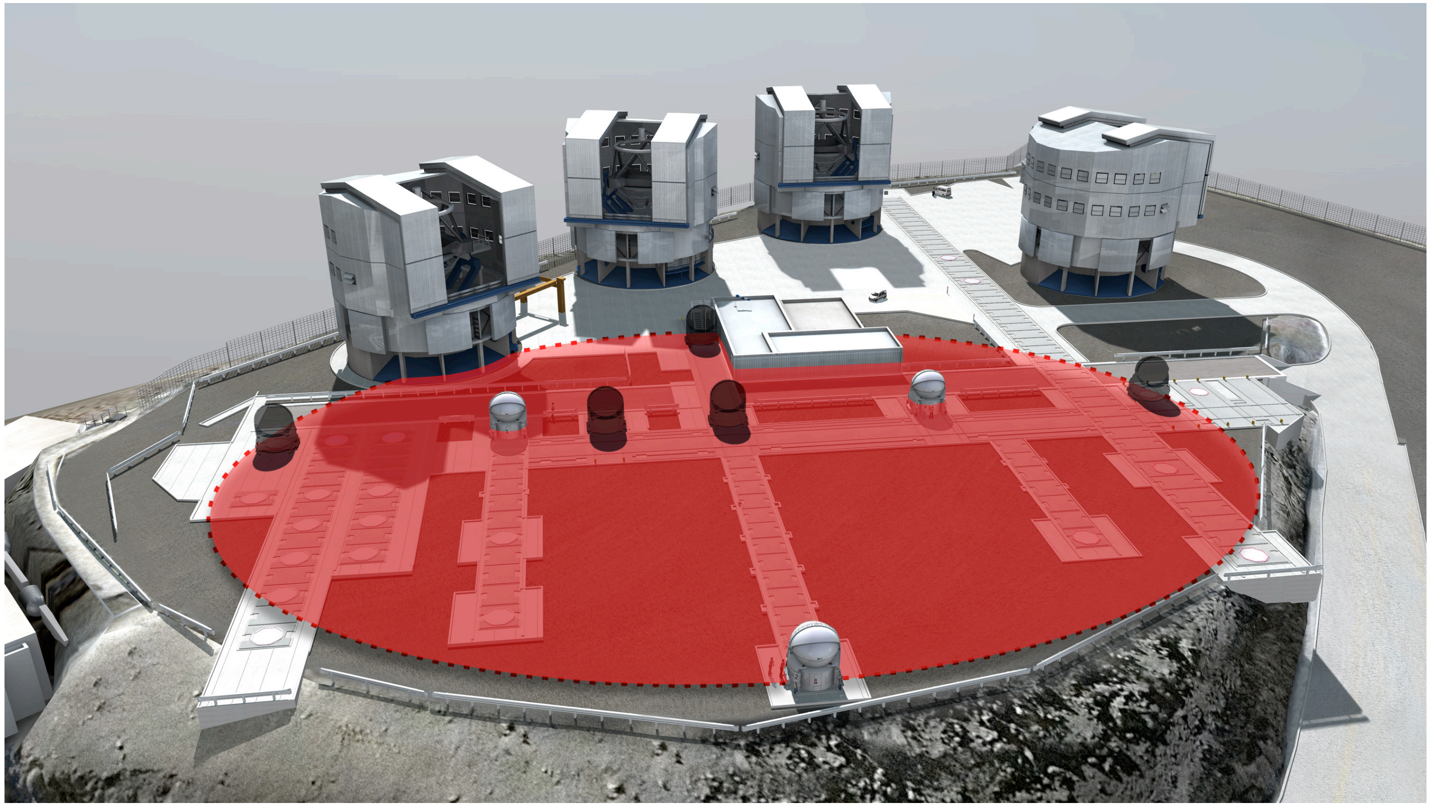

VLTI: A virtual 100-metre telescope

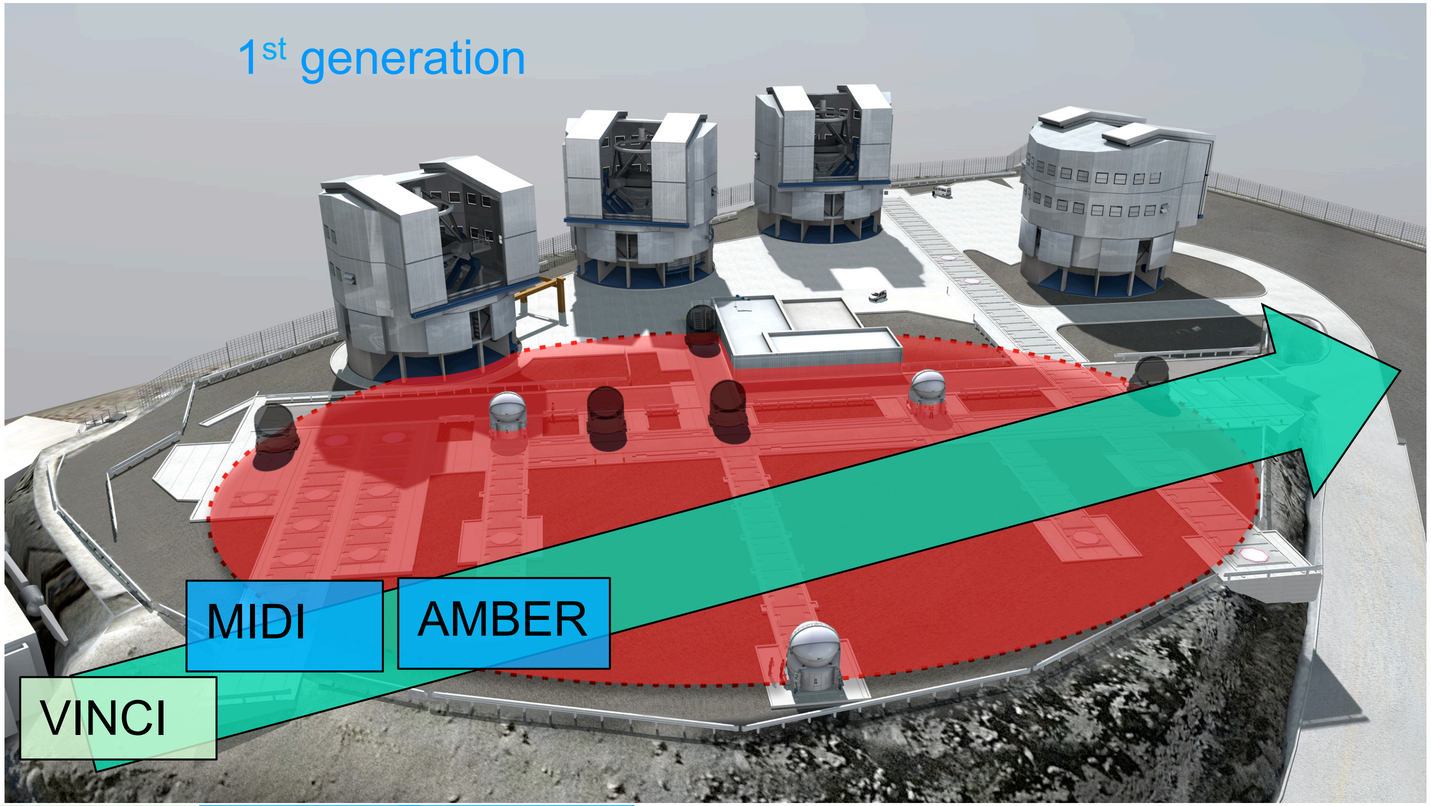

2001	2002-2015	2004
K-band (broad)	N-band	(J)HK-band
2-way beam comb.	2-way	3-way
(Test) Instrument	*R*=30,230	*R*=30,1500, 12000
High-precision		

VLTI: A virtual 100-metre telescope

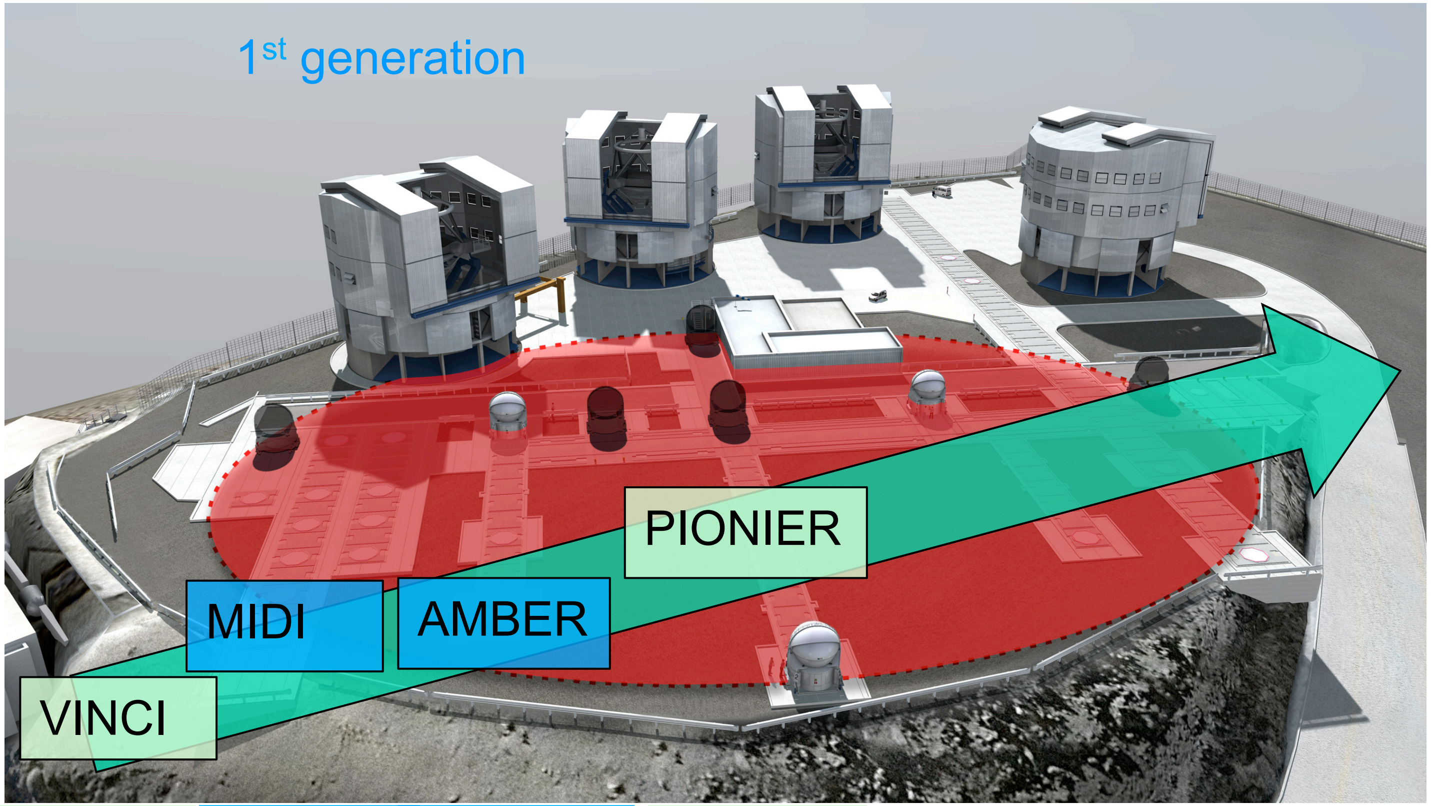

2001	2002-2015	2004	2010/2015
K-band (broad)	N-band	(J)HK-band	H(K)-band
2-way beam comb.	2-way	3-way	4-way
(Test) Instrument	*R*=30,230	*R*=30,1500, 12000	*R* ~20
High-precision			

VLTI: A virtual 100-metre telescope

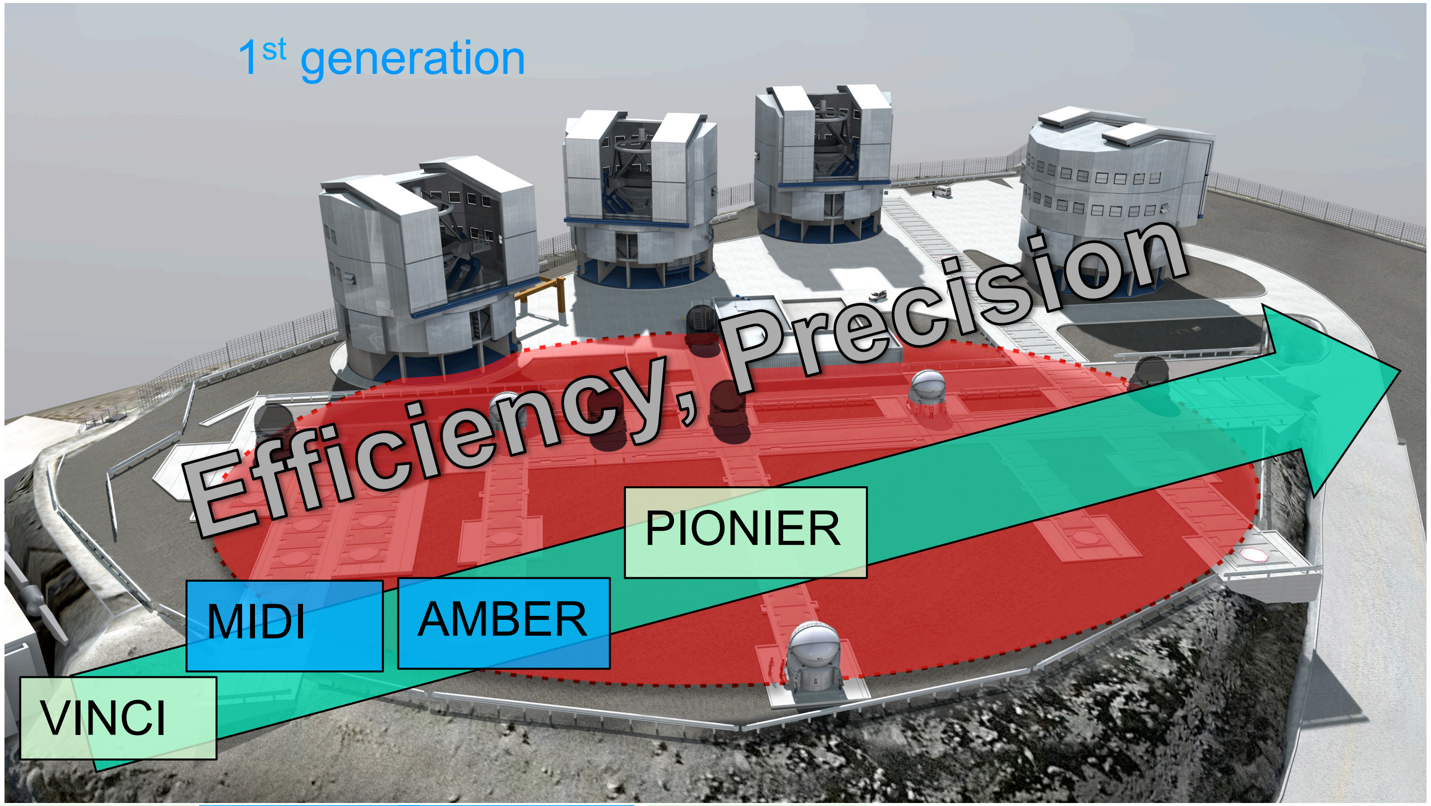

2001 K-band (broad) 2-way beam comb. (Test) Instrument High-precision	2002-2015 N-band 2-way *R*=30,230	2004 (J)HK-band 3-way *R*=30,1500, 12000	2010/2015 H(K)-band 4-way *R* ~20

VLTI: A virtual 100-metre telescope

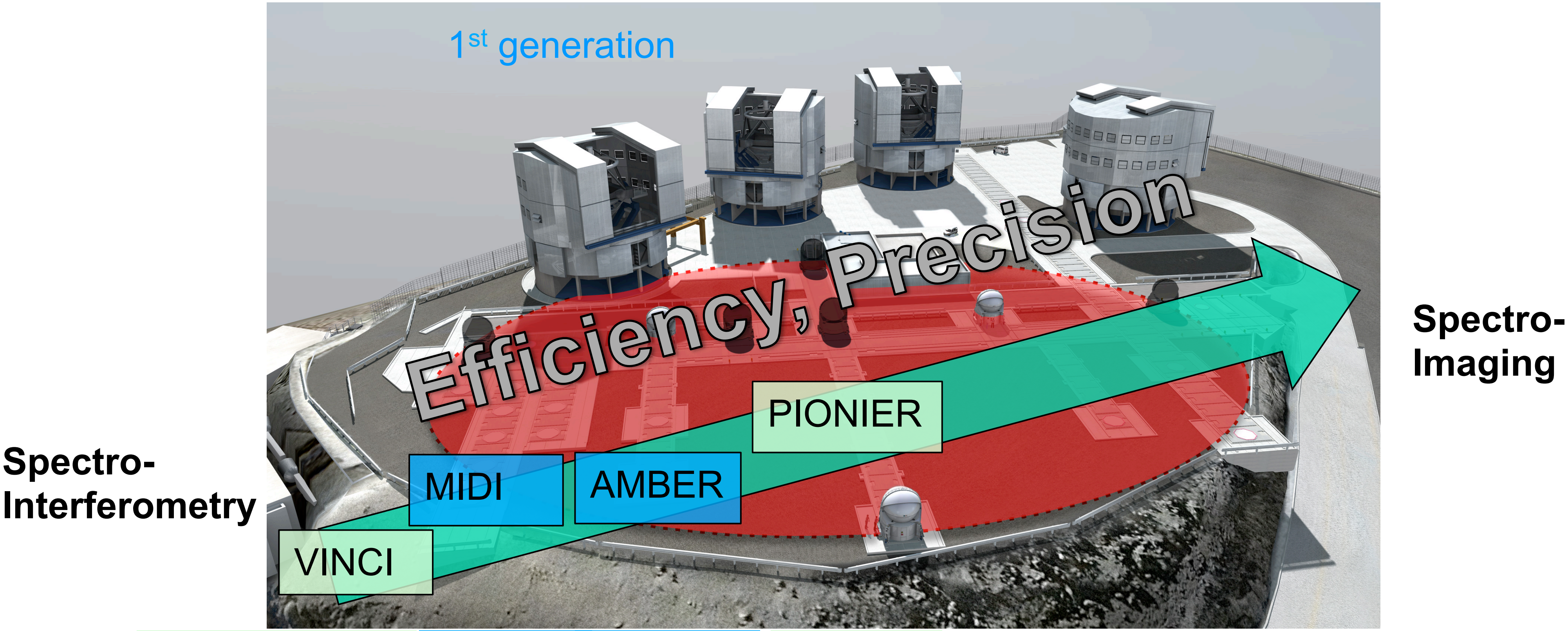

2001	2002-2015	2004	2010/2015
K-band (broad)	N-band	(J)HK-band	H(K)-band
2-way beam comb.	2-way	3-way	4-way
(Test) Instrument	*R*=30,230	*R*=30,1500, 12000	*R* ~20
High-precision			

VLTI: A virtual 100-metre telescope

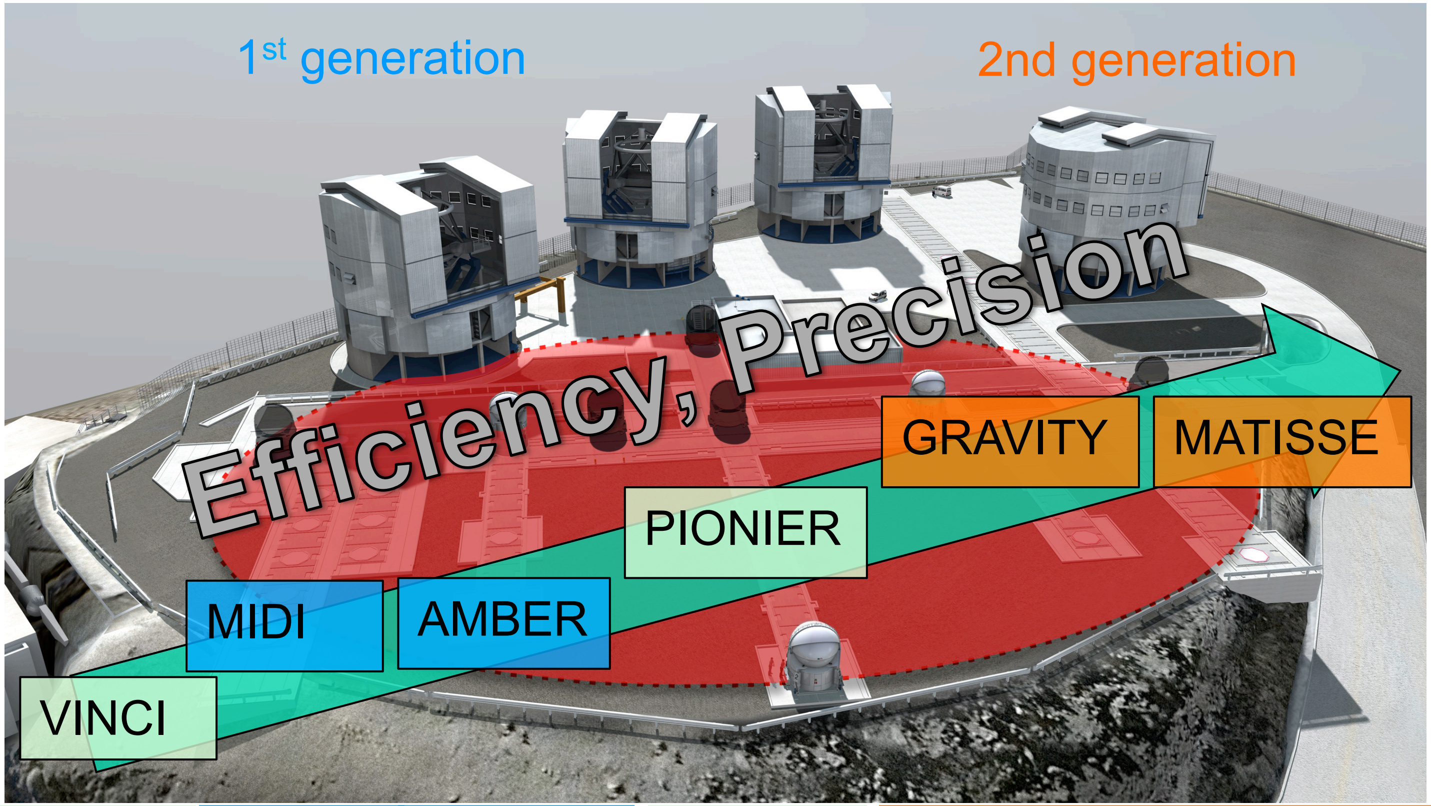

Spectro-Interferometry

Spectro-Imaging

2001 K-band (broad) 2-way beam comb. (Test) Instrument High-precision	2002 N-band 2-way *R*=30,230	2004 (J)HK-band 3-way *R*=30,1500, 12000	2010/2015 H(K)-band 4-way *R* ~20	2015 (?) K-band 4-way *R*~22, 500, 4000 Astrometry High-precision	(2016+?) LMN-band 4-way *R*~30, 450/200 High-precision

Sketch of an oxygen-rich Mira star

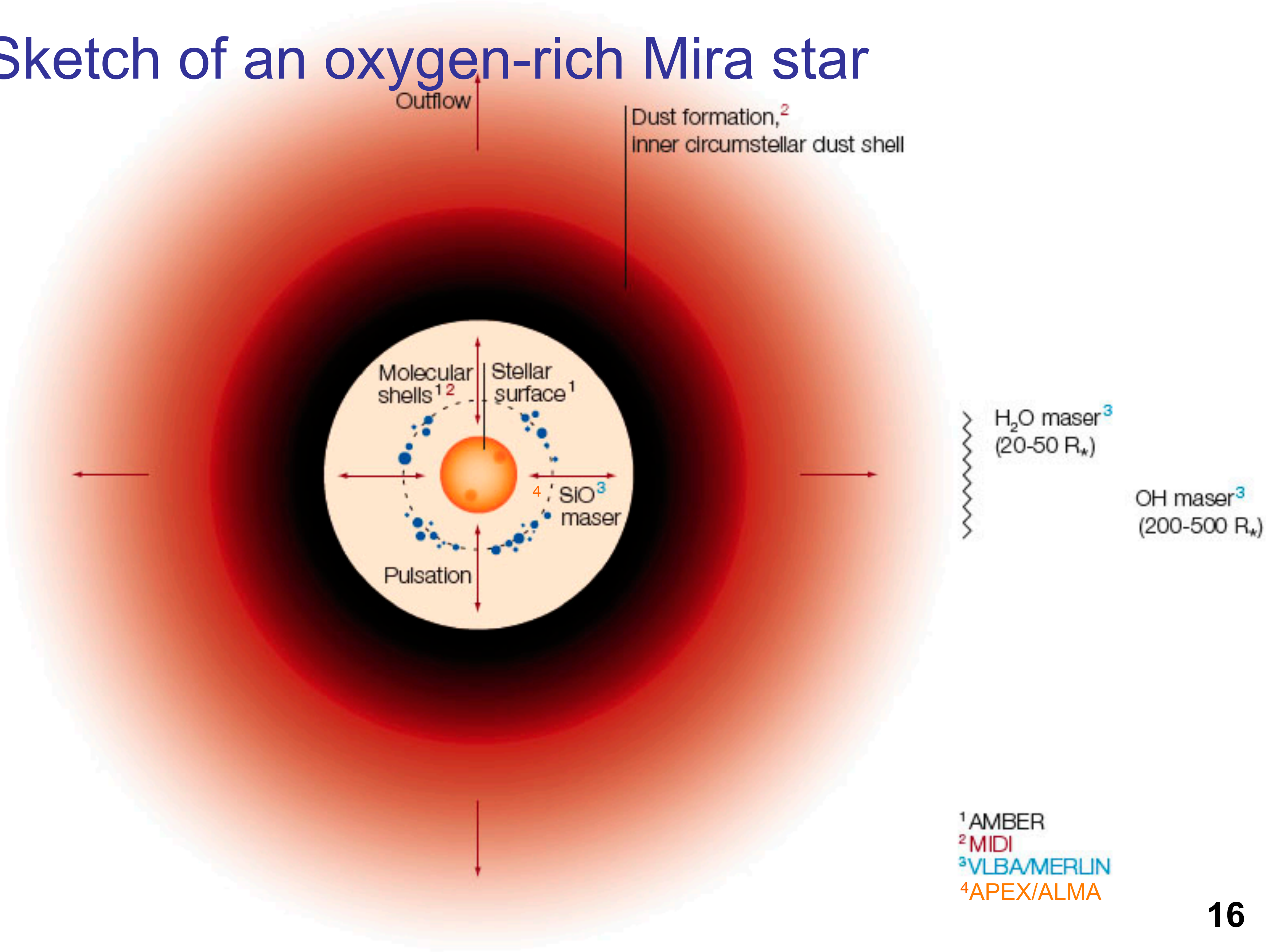

Outline

- Molecular layers of AGB stars and their extension
  - Oxygen-rich Miras
  - Oxygen-rich semi-regular AGB star
  - Oxygen-rich OH/IR stars
  - Carbon-rich semi-regular AGB star
- Molecular layers of red supergiants and their extension
- Dust formation of oxygen-rich Miras

Molecular layer scenario - Traditions

- Tsuji (2001) and earlier: Based on ISO data: “We confirm that a rather warm molecule forming region should exist as a new M giant component of the atmosphere of red giant stars and that this should be a general phenomenon in late-type stars” – “MOLsphere”
- Bessel, Scholz, Wood (1996); Hofmann, Scholz, Wood; Hofmann, Scholz (1998) and earlier: non-Mira and Mira M giant models: Dynamic model atmospheres of M giants naturally produce extended molecular layers in agreement with observed spectra
- Similar for dynamic atmospheres of carbon stars
- *Narrow-band* interferometry with IOTA of a Mira star and a RSG by Perrin et al. (2004, 2005) confirmed the molecular layer scenario by spatially resolved observations.

Cool evolved stars: Molecular shell scenario

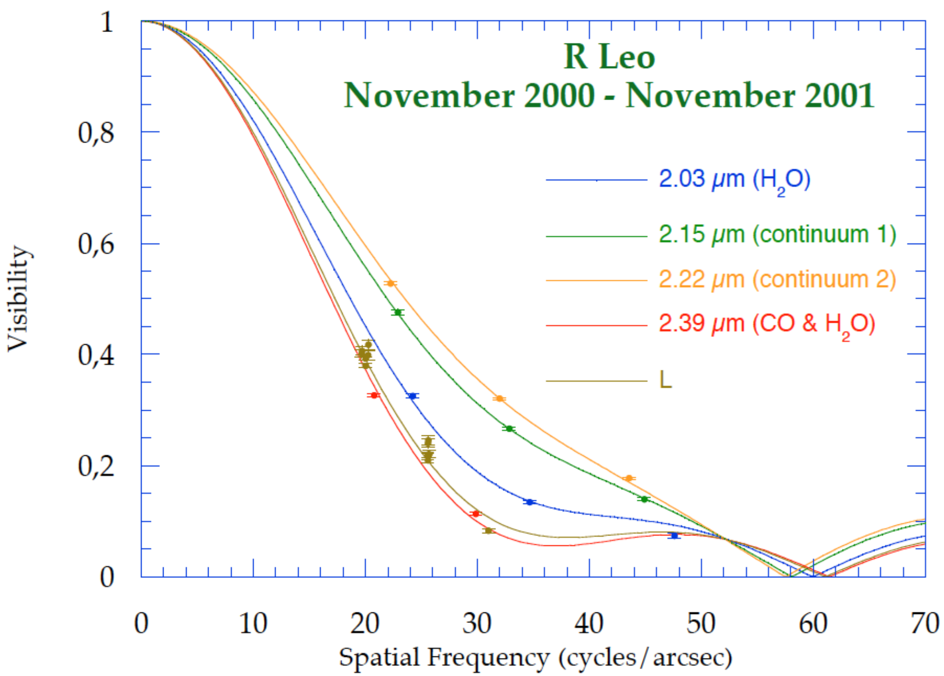

Perrin et al. (2004)

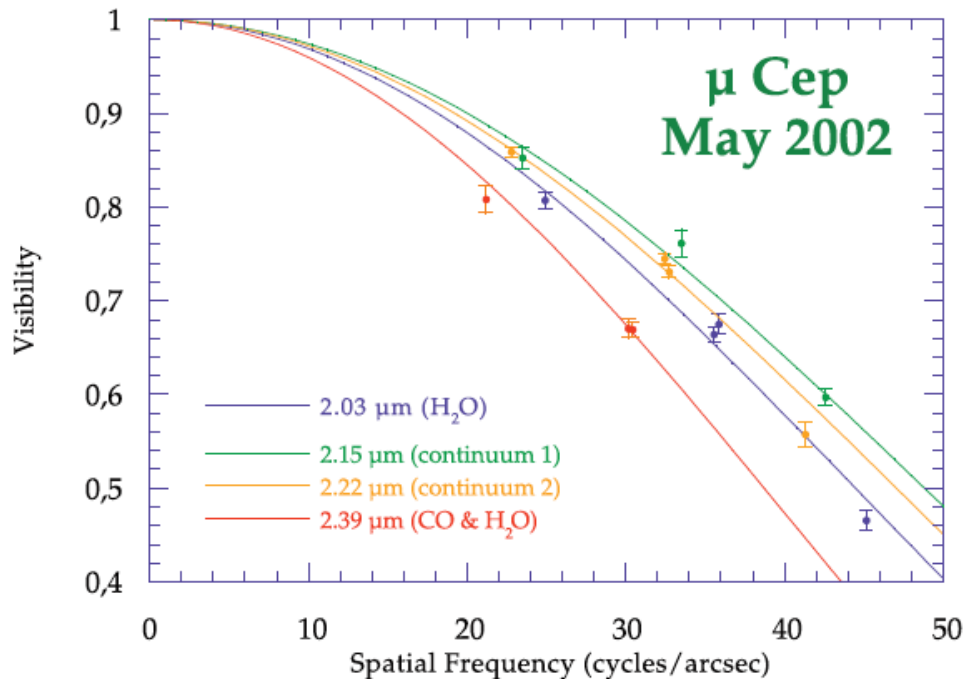

Perrin et al. (2005)

Narrow-band interferometry with IOTA of a Mira star (left) and a RSG (right) by Perrin et al. (2004, 2005).

It is established that both Mira stars and RSG stars are surrounded by molecular layers.

Asymmetric water shells in Miras

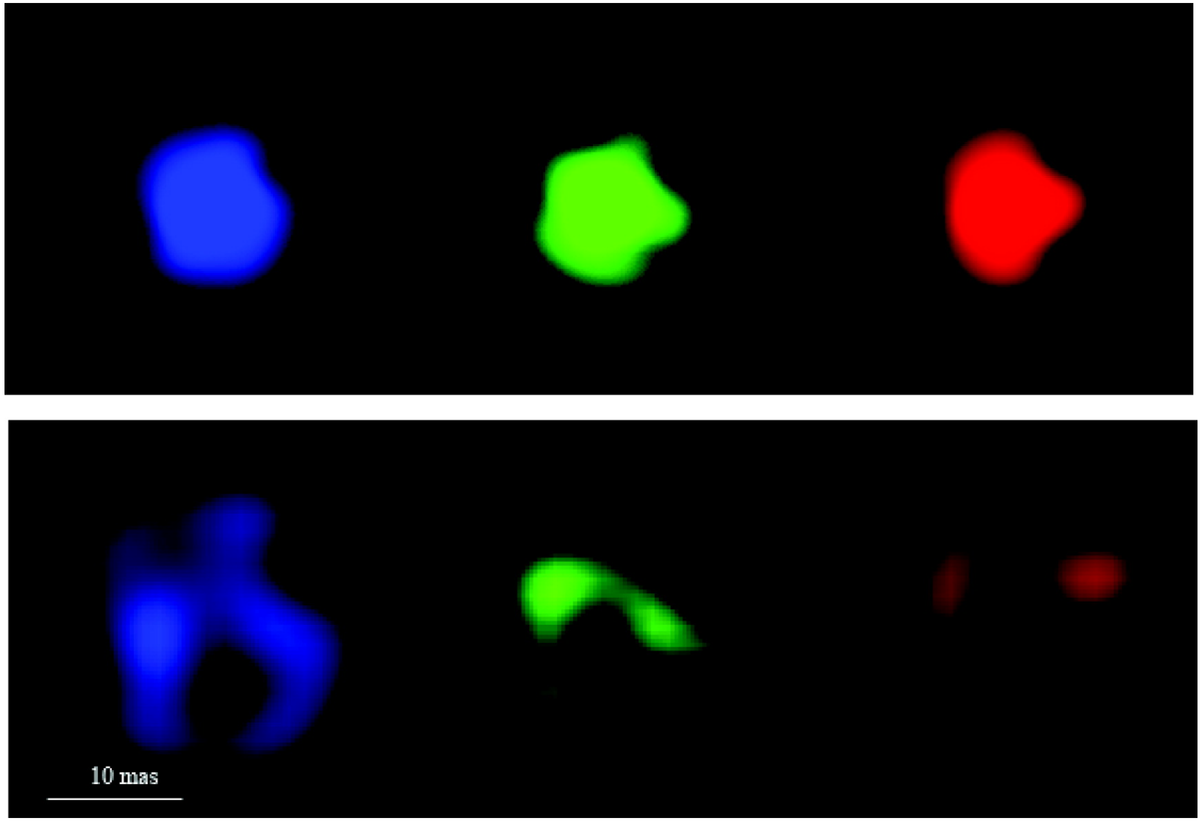

Ragland et al. 2008, IOTA observations of R Aqr: "Reconstructed near-infrared images of R Aqr. The blue, green, and red color images (from left to right) represent 1.51, 1.64, and 1.78 μm respectively. The top row shows reconstructed images, and the bottom row shows primarily contributions from the shell, since we subtracted a Gaussian function from the reconstructed images to remove the stellar component."

Ragland et al. 2008

VLTI/AMBER OBSERVATIONS OF AGB STARS: MOLECULAR LAYERS

AMBER spectro-interferometry: Mira stars

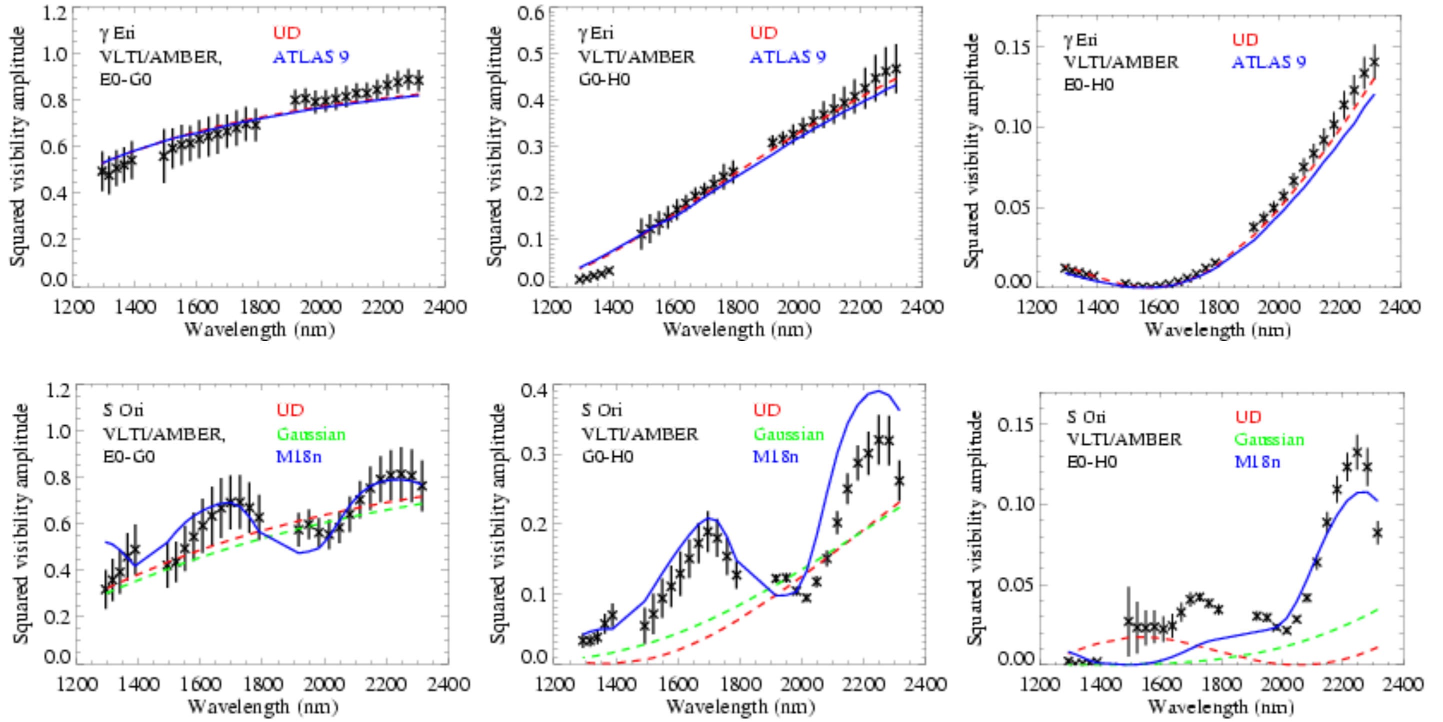

M giant

Mira

The bumpy visibility curve is a signature of molecular layers lying above the photosphere.

At some wavelengths, the molecular opacity is low, we see the photosphere, the target appears smaller.

At other wavelengths, the molecular opacity is larger, we see the water shell, the target appears larger.

AMBER allows us to probe different layers of the extended atmosphere.

Visibility and UD diameter variations with wavelength resemble reasonably well the predictions by dynamic model atmospheres including molecular layers, in particular water vapor and CO.

Wittkowski, et al. 2008

Mira stars and pulsation models

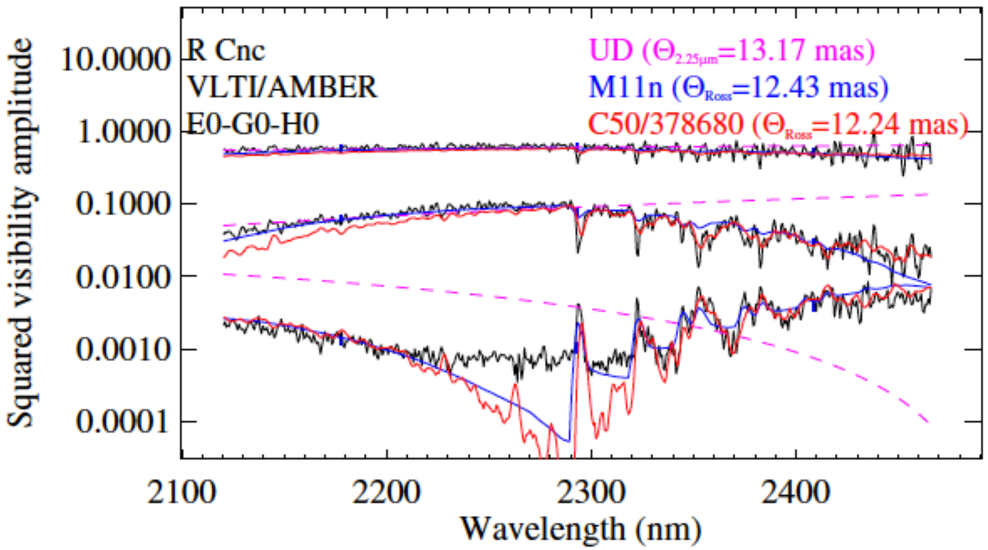

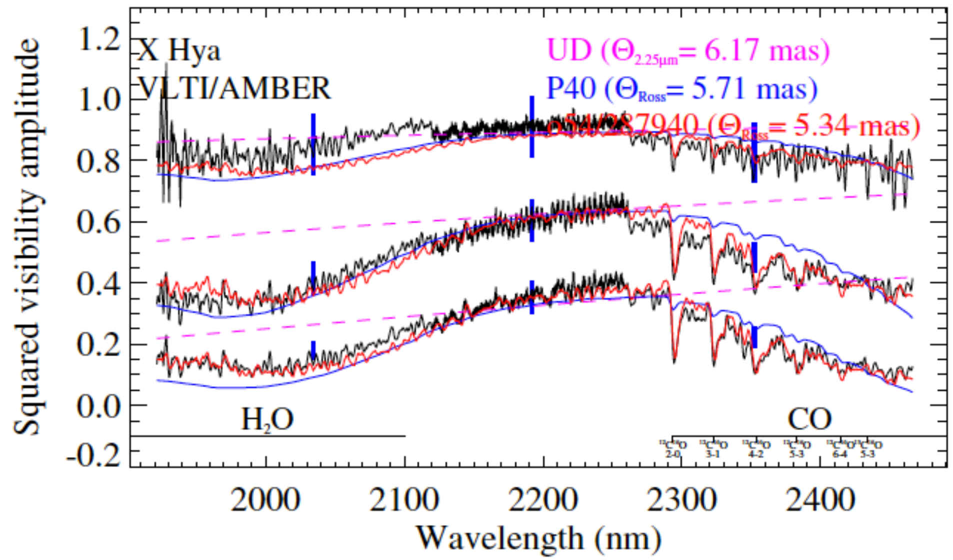

Visibilities are well consistent with predictions by the latest dynamic model atmosphere series based on self-excited pulsation models and including atmospheric molecular layers (CODEX models by Ireland, Scholz, & Wood 2008, 2011). However, these models do not yet explain an outflow/mass loss.

Best-fit parameters (phase, T_{eff}, distances) consistent with independent estimates. Teff also determined from best-fit angular diameter and simultaneous SAAO photometry.

Wittkowski et al. 2011

Wavelength-dependent closure phases

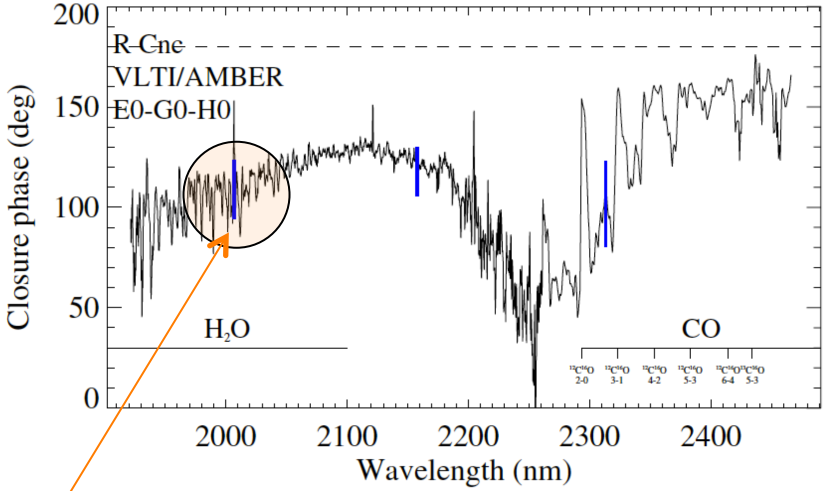

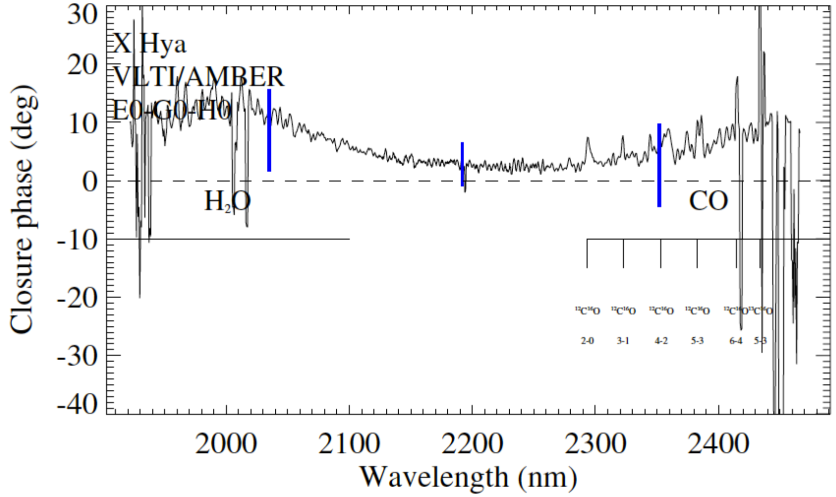

For example, one unresolved spot at separation 4 mas contributing 3% of the total flux

Wavelength-dependent closure phases indicate deviations from point symmetry at all wavelengths and thus a complex non-spherical stratification of the atmosphere. In particular, the strong closure phase signal in the water vapor and CO bandpasses is interpreted as a signature of large-scale inhomogeneities/clumps of molecular layers.

These might be caused by pulsation- and shock-induced chaotic motion in the extended atmosphere as theoretically predicted by Icke et al. (1992) and Ireland et al. (2008, 2011).

Wittkowski et al. 2011

VLTI/AMBER two-epoch imaging of the Mira X Hya

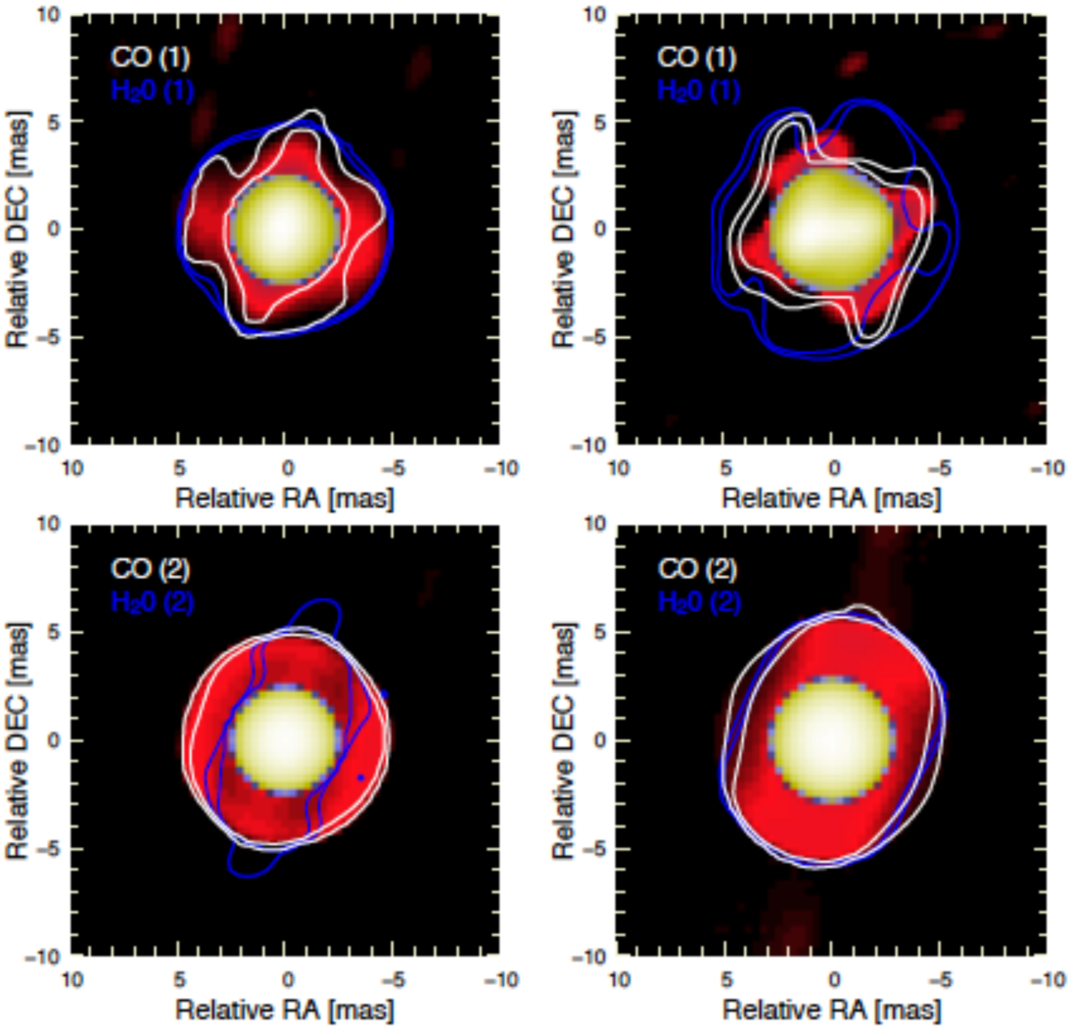

Fig. 16. Continuum images overplotted (Fig. 13) with H_2O (blue) and CO (white) intensity contours (from Figs. 14 and 15). Intensity contour levels represent 2% and 5% of the maximum intensity of each image and allow to compare the extension and shape of the environment between spectral bands for Epoch A (left panels) and B (right panels). Upper panels represent the Cont (1), H_2O(1) and CO(1) bands whereas the lower panels represent the Cont (2), H_2O(2) and CO(2) bands.

- Angular scale change between phase 0.0 and 0.2
- 1D CODEX profiles consistent with spectral variation of squared visibilities
- Reconstructed model-dependent images reproduce closure phase, showing phase-dependent material inhomogeneities located in the atmospheric molecular layers

Haubois et al. 2015

Time variability of R Cnc

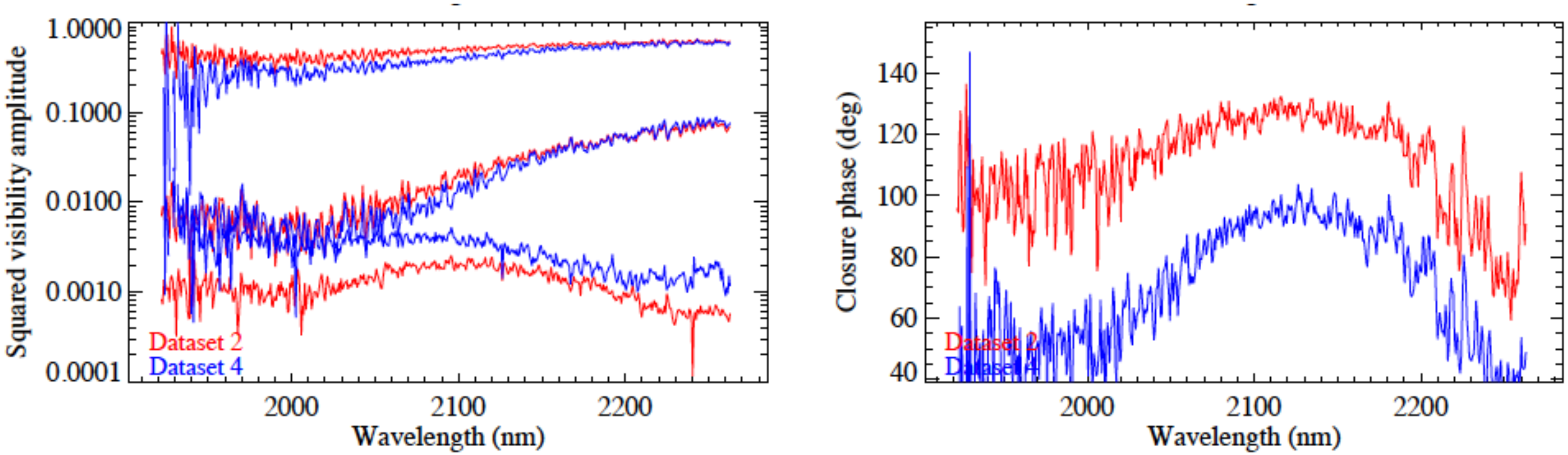

2 epochs of R Cnc separated by about 2 months at phases 0.3 and 0.5:

- Marginal variability at high visibilities (overall structure)
- Clear variability at low visibilities and closure phases (detailed structure)

Wittkowski et al. in prep

VLTI/AMBER MR observations of the semi-regular pulsating AGB star RS Cap

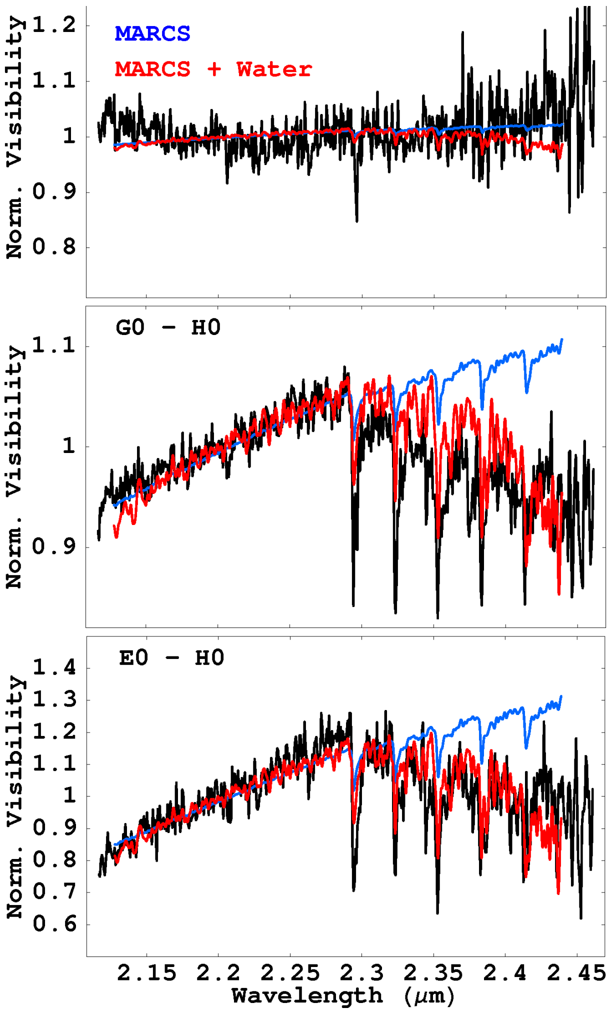

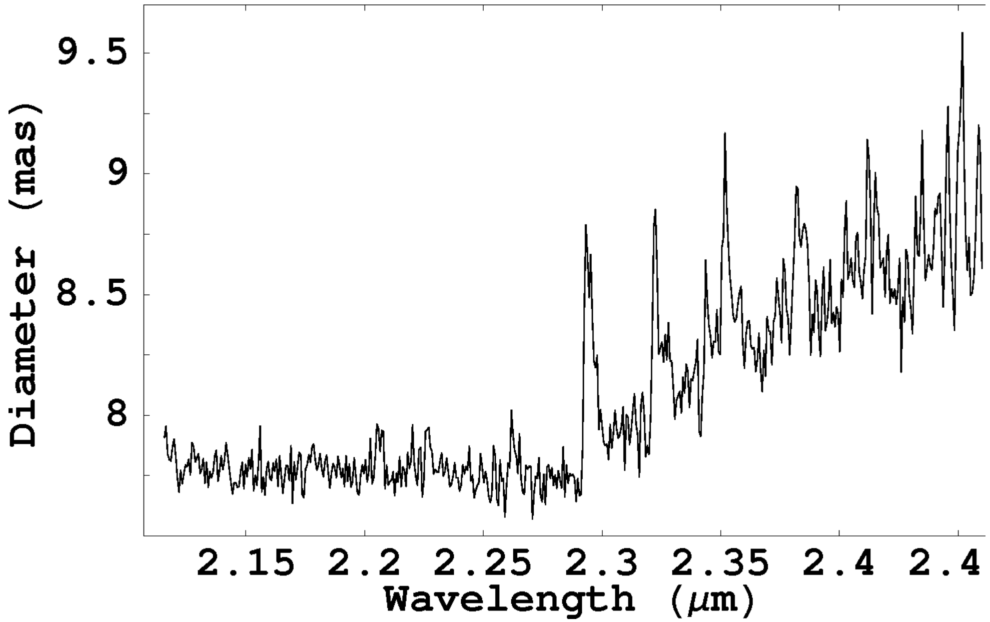

Marti-Vidal et al. 2011

VLTI/AMBER observations of three OH/IR stars

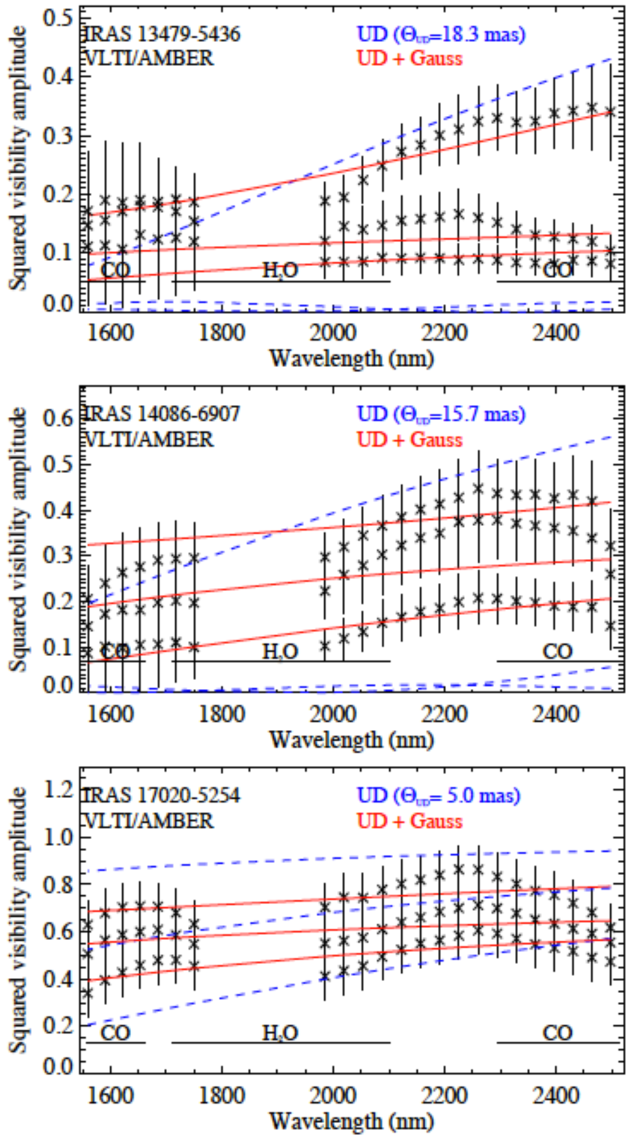

Detection of spectral visibility variations that resemble those of S Ori and other AGB stars and that coincide with the positions of CO and H_2O bands.

Single component model does not fit the data. Simple two-component model (UD+Gauss) results in stellar components of 3-5 mas (900-1400 R_{sun}) and CS dust shell components of 17-25 mas (9000-13000 R_{sun}), consistent with canonical properties of tip-AGB stars.

CS dust shell component is interpreted as the result Of the “superwind” phase. Different targets may represent different stages of the superwind and/or different stellar masses.

Ruiz-Velasco et al. 2011

1D Pulsation models versus 3D convection and pulsation models

Freytag & Höfner (2008): “The strong atmospheric shock waves associated with the giant convection cells lead to a levitation of the upper atmospheric layers in the 3D models. This is comparable to the effect of stellar pulsations – simulated by a variable membrane below the photosphere (piston) – in the 1D models.”

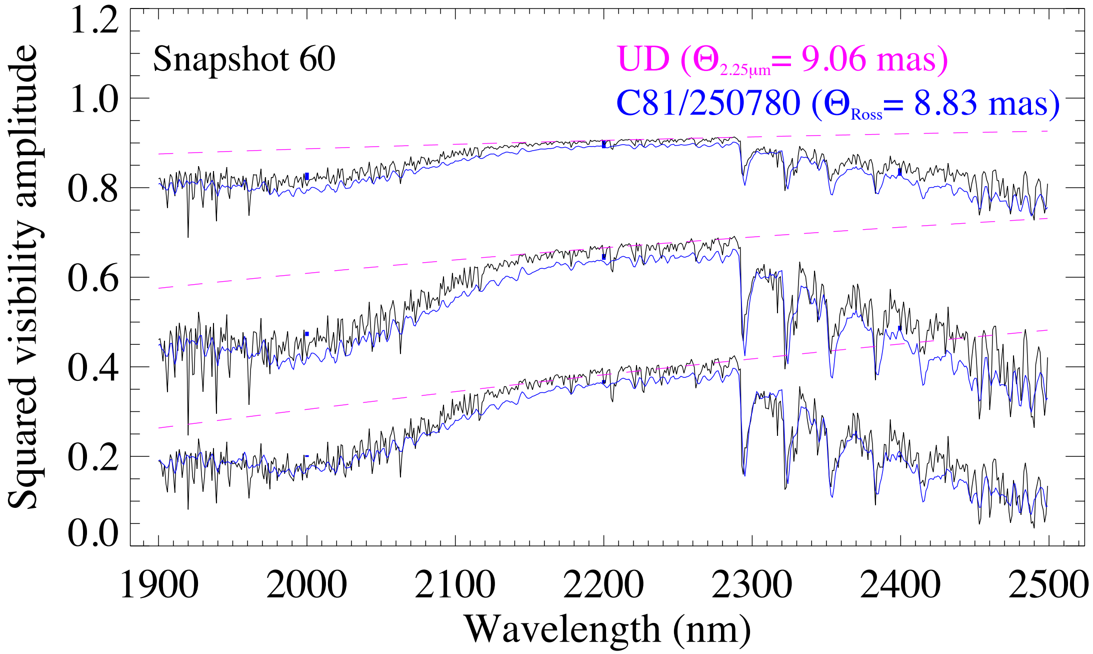

Indeed, synthetic visibility data from these 3D simulations are well consistent with those from CODEX 1D self-excited pulsation models.

Chiavassa/Wittkowski, in progress

Observations compared to 1D and 3D models

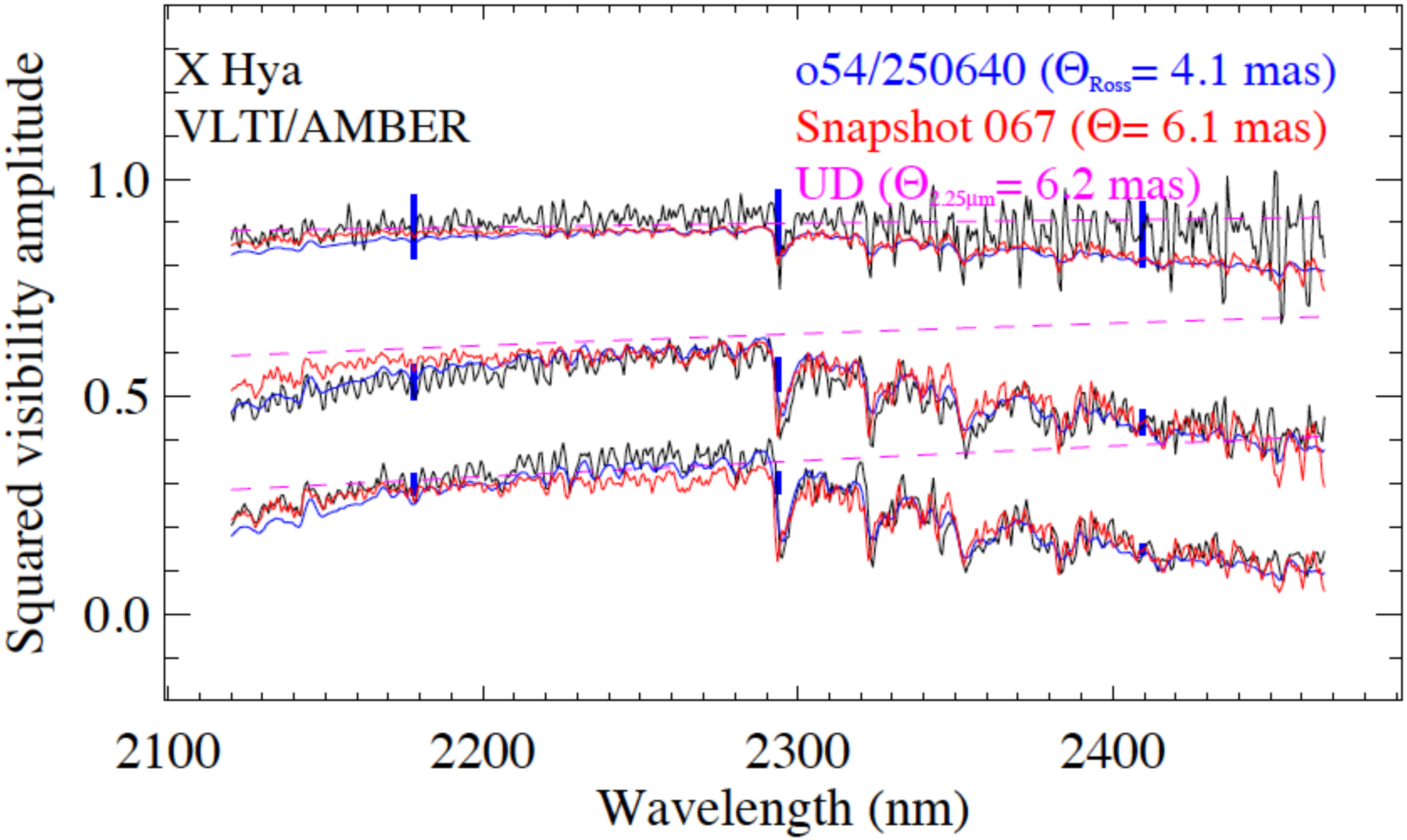

Wittkowski et al. in prep

Water band

Near-continuum

CO (2-0) bandhead

CO (+Water) band

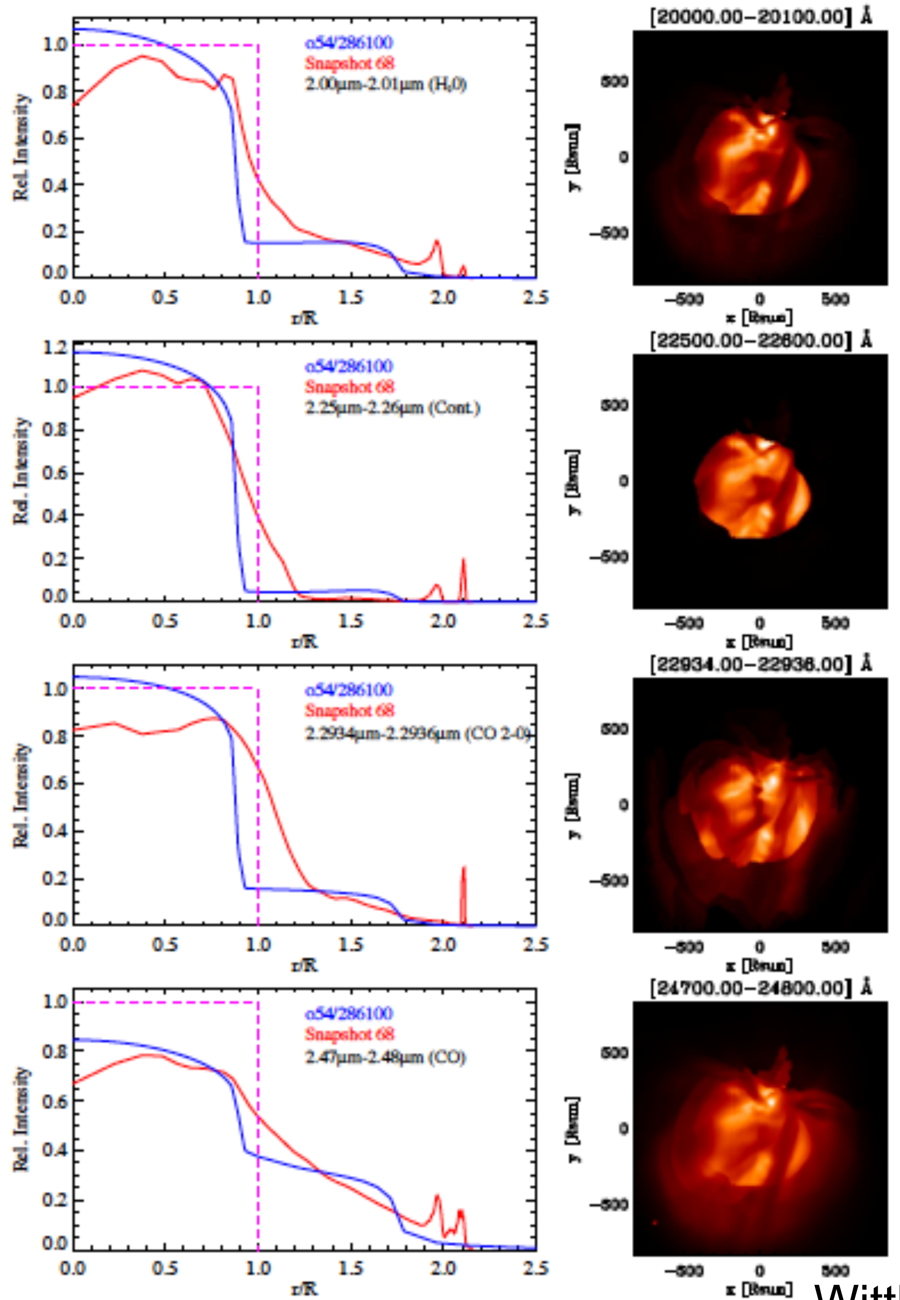

Wittkowski et al. in prep

Miras: Fundamental parameters

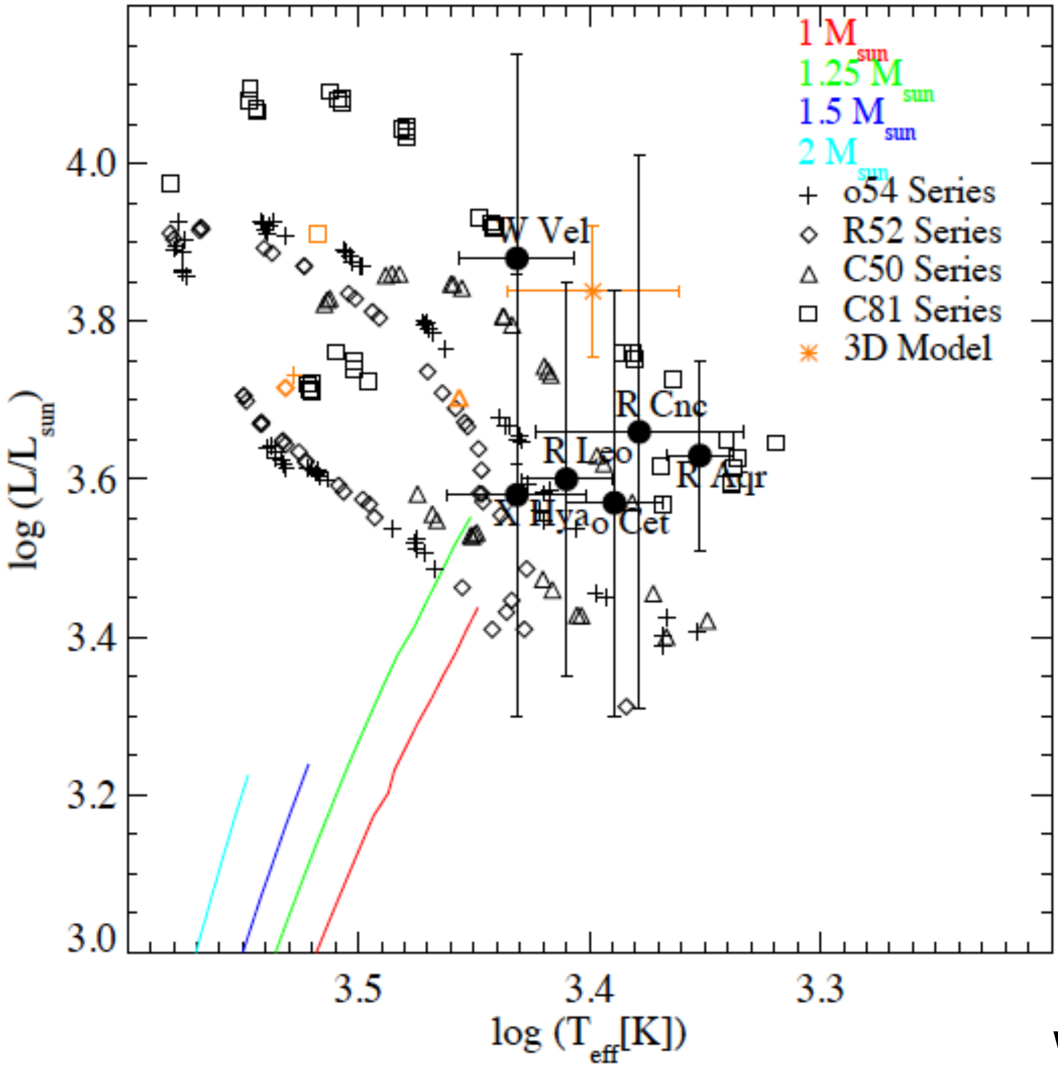

Wittkowski et al. in prep

R Scl: ALMA Cycle 0 band 7 CO(3-2)

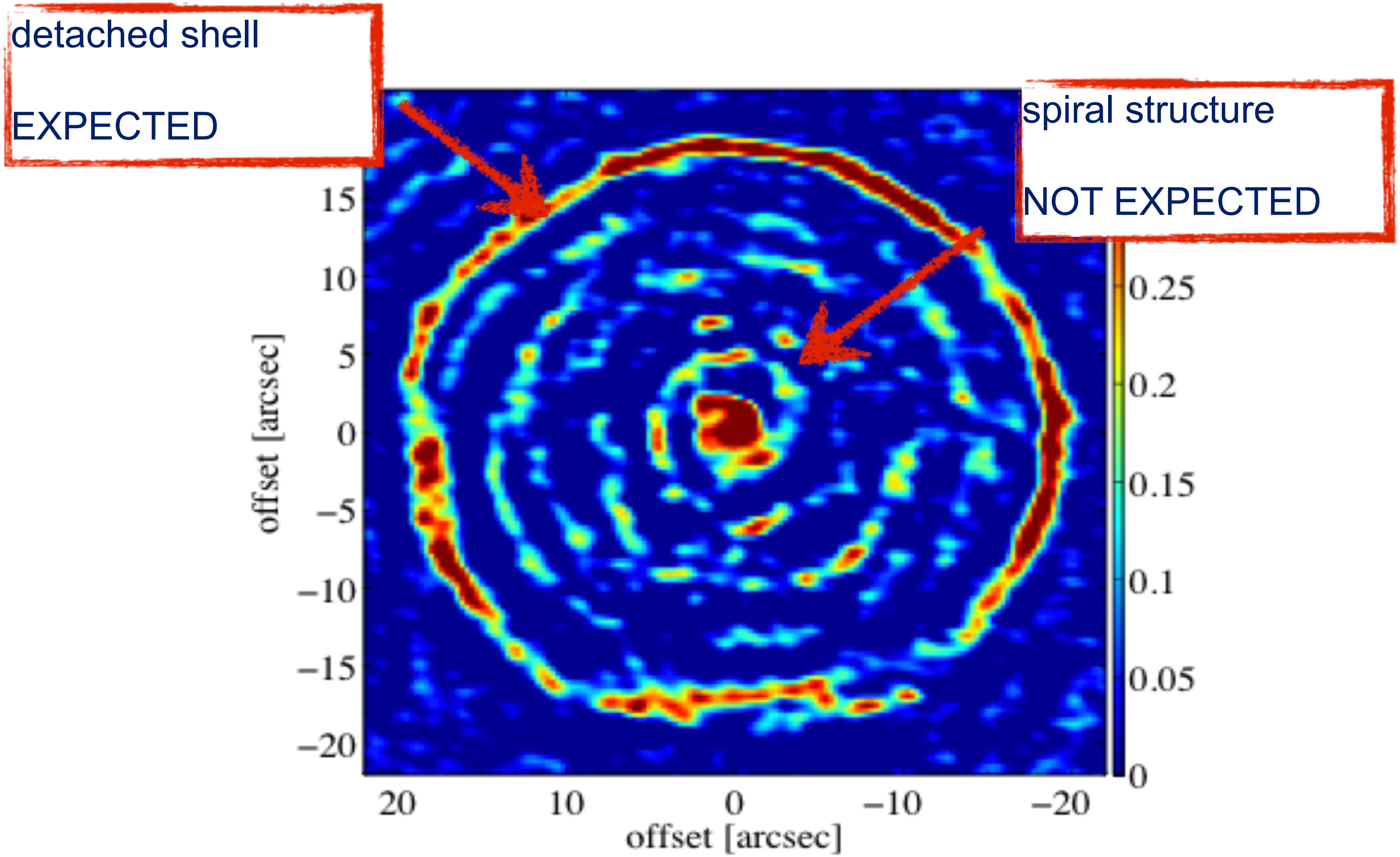

Maercker et al. 2012

VLTI/PIONIER image of R Scl

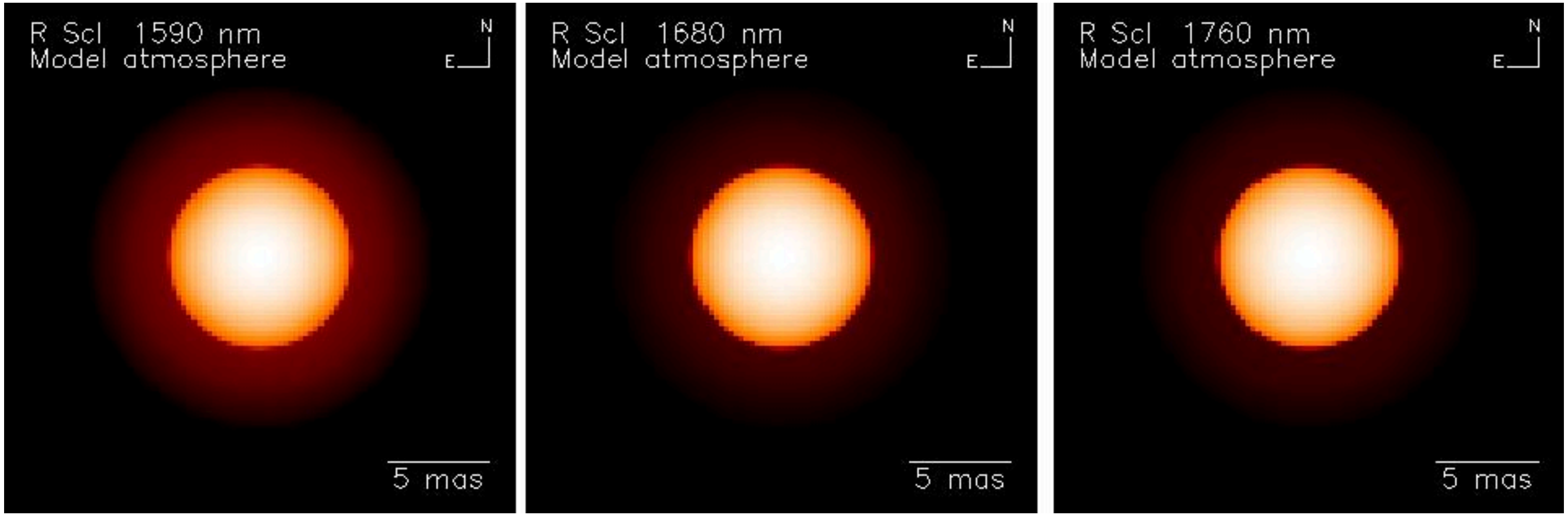

Best-fit model atmosphere predictions based on the
carbon star grid by Mattsson et al. 2010; Eriksson et al. 2014).
Note that the best-fit model does not have a mass loss.

Wittkowski et al., in prep

VLTI/PIONIER image of R Scl

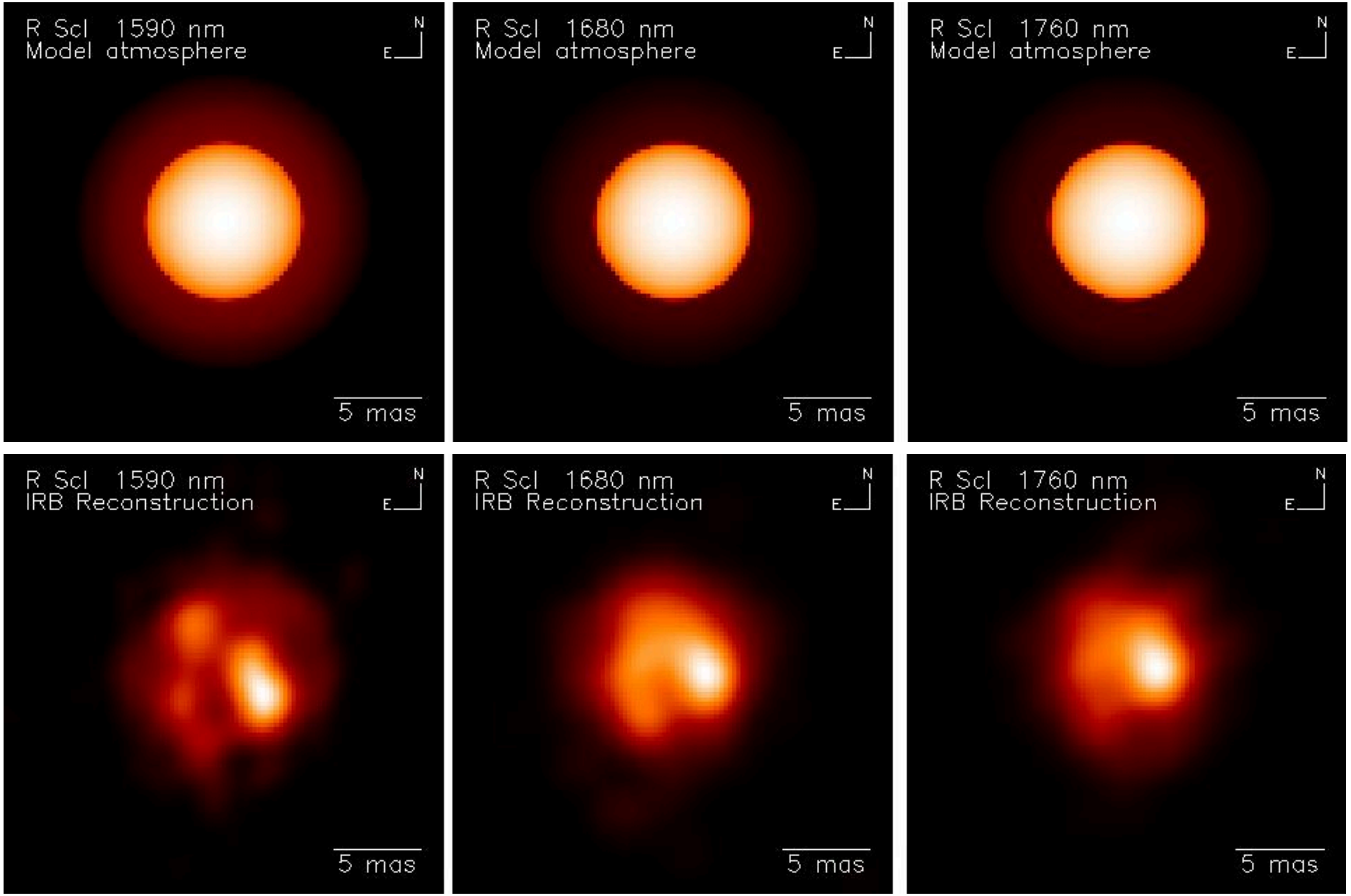

Wittkowski et al., in prep

VLTI/AMBER OBSERVATIONS OF RED SUPERGIANTS: MOLECULAR LAYERS

VLTI/AMBER observations of the red supergiant VX Sgr

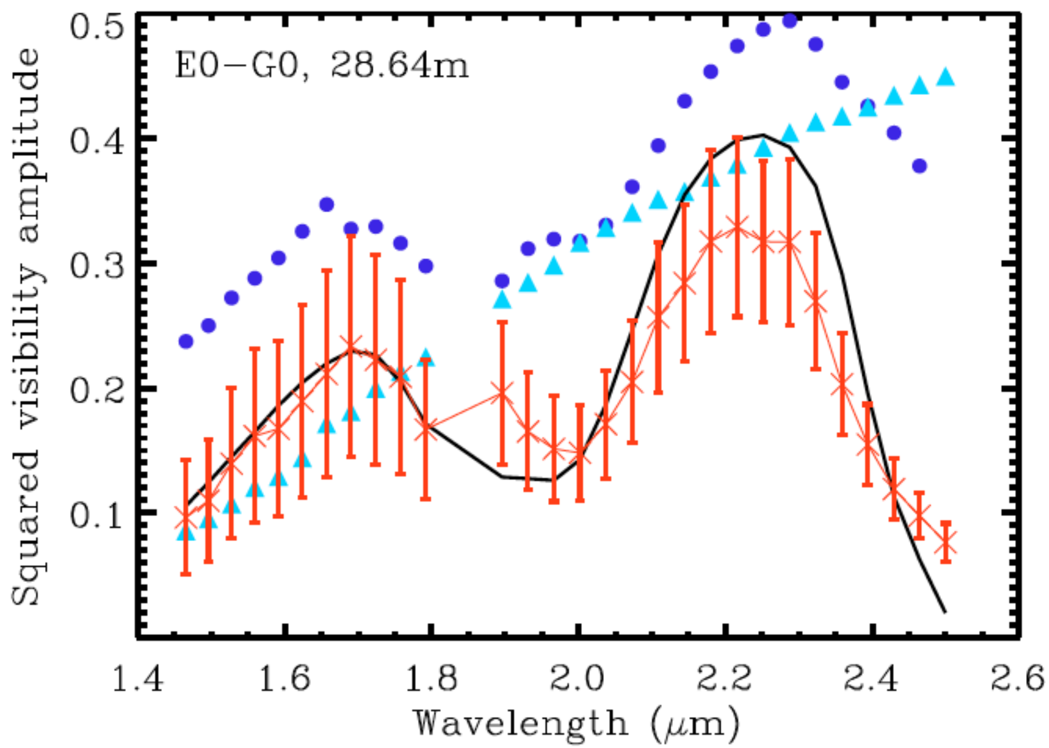

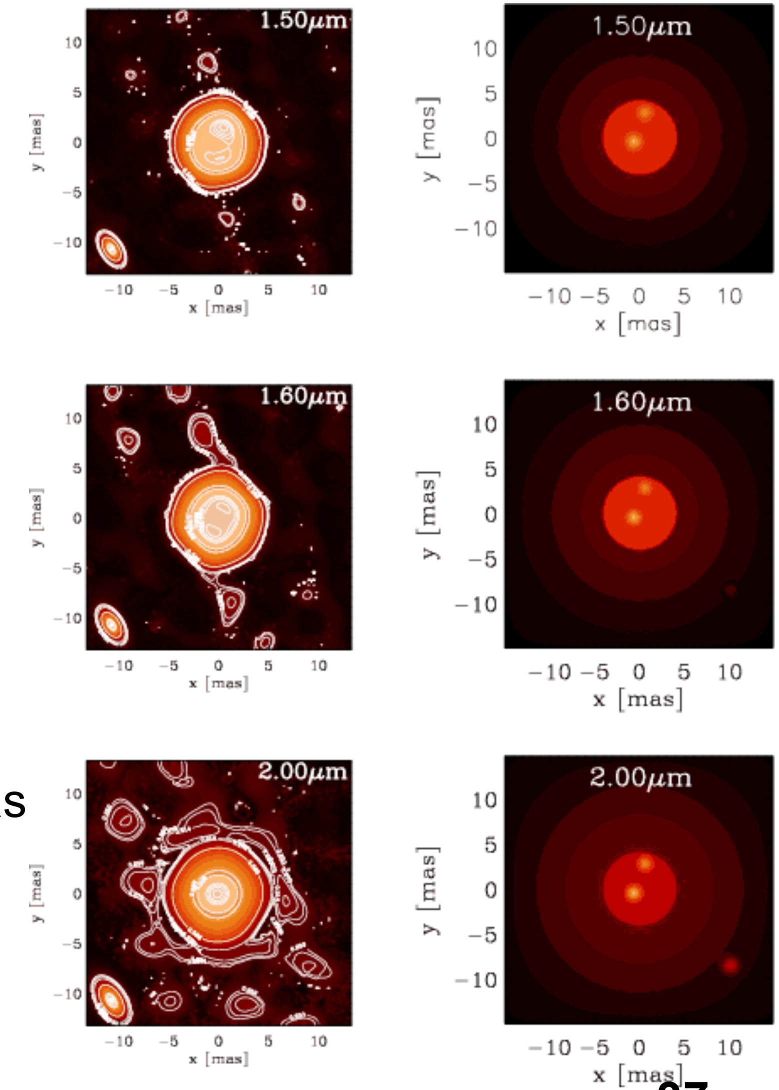

- Visibility shape versus wavelength as seen for Miras
- Consistent with 1D pulsation models and 3D convection simulations of **AGB** stars
- Shape is not re-produced by 3D models of RSGs

Chiavassa et al. 2010

Chiavassa et al. 2010

AMBER spectro-interferometry: RSGs

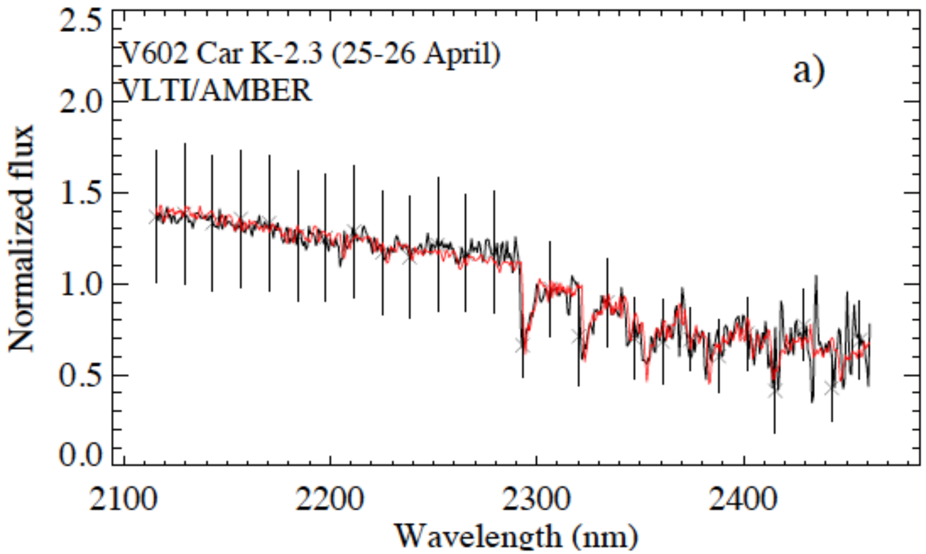

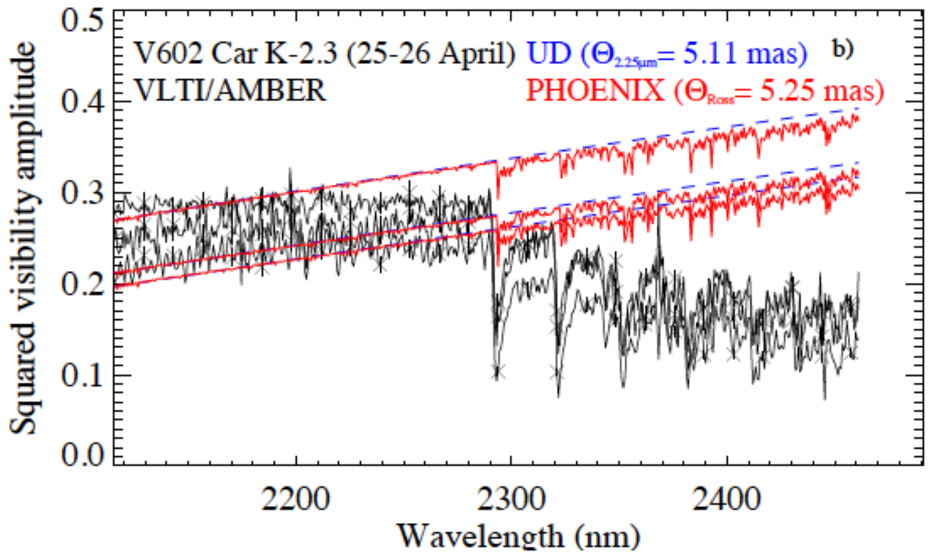

The PHOENIx model atmospheres reproduce the spectra fairly well,
but do not predict the drops of the visibility in the water vapor and CO bands.

This means that the molecular opacities are included, but that the models are too compact compared to our observation.

Arroyo-Torres et al. 2013; 2015

RSGs: Atmospheric extension versus luminosity

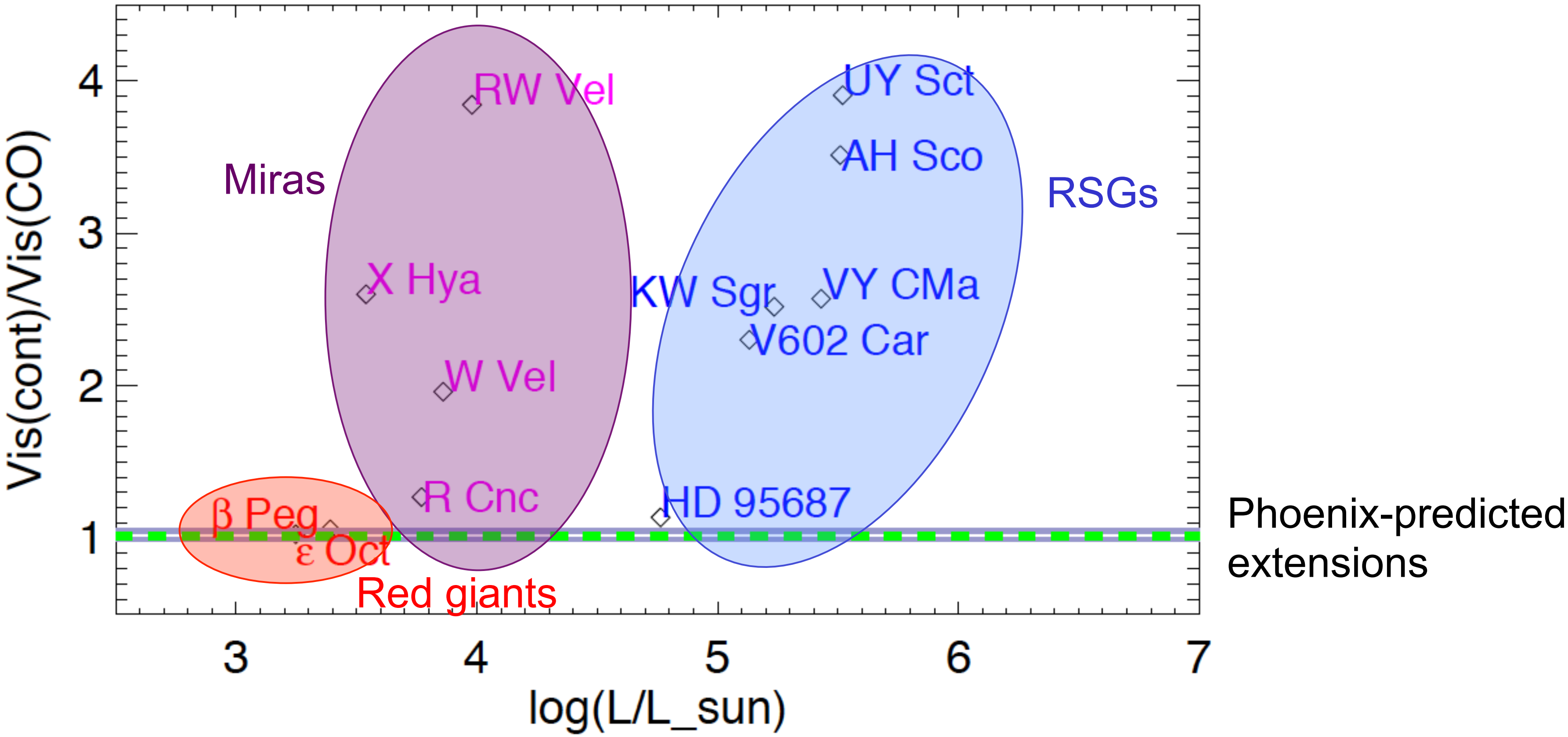

RSG stars and Mira stars have similar atmospheric extensions.

Mira model extensions are of the order of 2-3 photospheric radii.

Arroyo-Torres et al., 2015

RSGs: Atmospheric extension versus luminosity

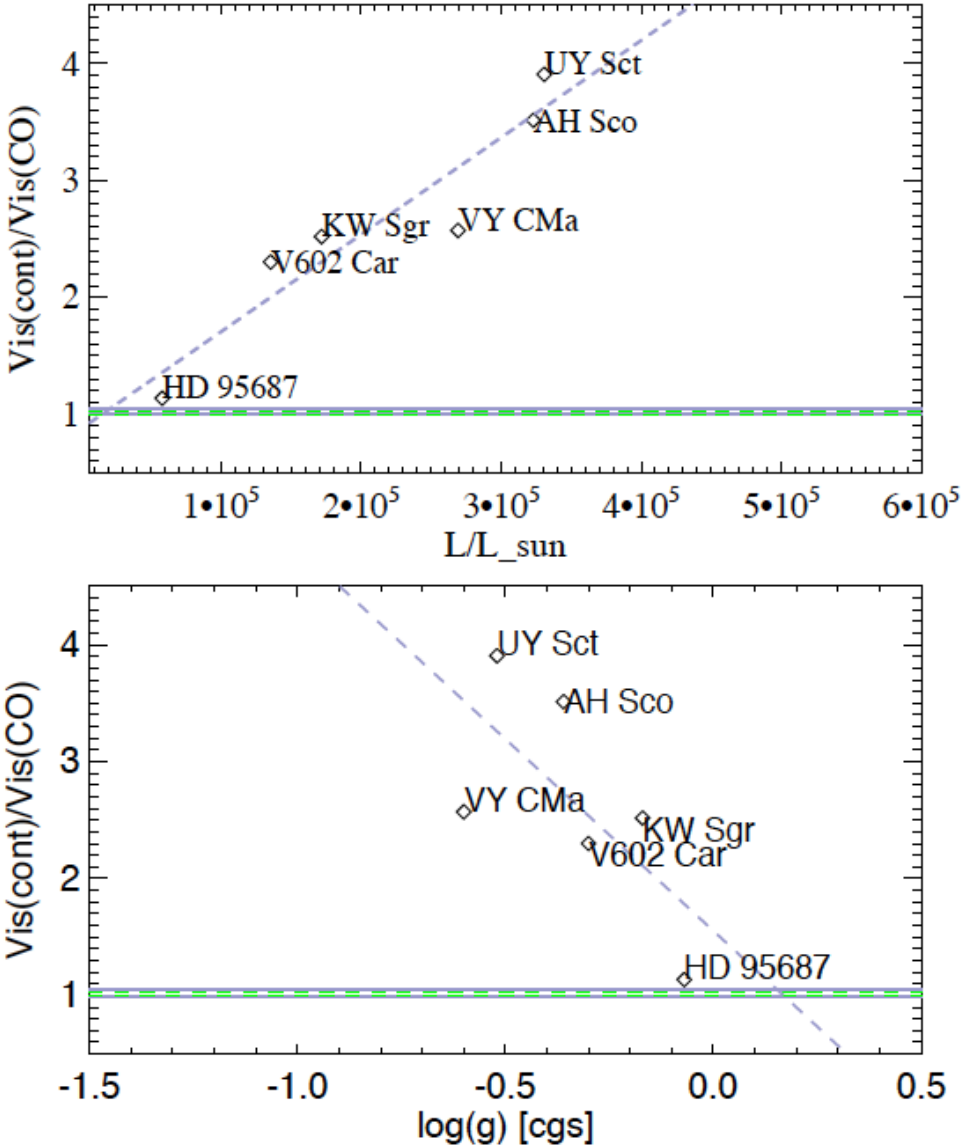

- The atmospheric extension of RSGs (based on the 1st CO bandhead) increases with increasing luminosity and decreasing surface gravity
- This correlation is not observed for Miras, pointing to a different physical mechanism
- Considerable extensions are only observed for luminosities above about 10^5 L_{sun} and below log g ~ 0.0

Arroyo-Torres et al., 2015

Comparison to convection models

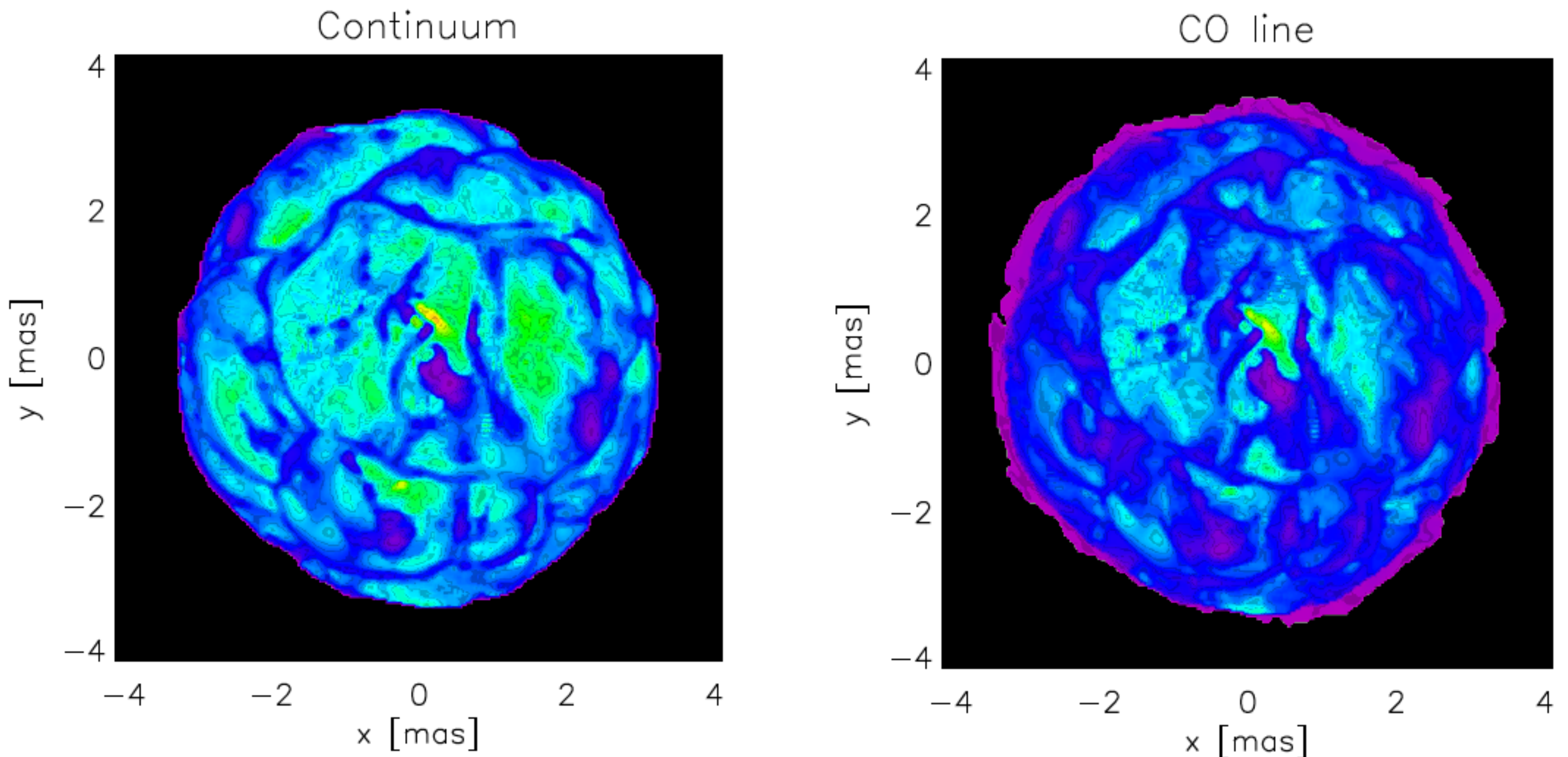

Teff=3487 K, log(g)=-0.335, R=830 $R_{\odot}$, M=12 $M_{\odot}$

The detailed surface structure in the CO line intensity map appears less corrugated and the details (eg.,intergranular lanes) almost disappear. The CO line surface looks slightly more extended (purple color close to the stellar limb).

Arroyo-Torres et al., 2015

Comparison to convection models

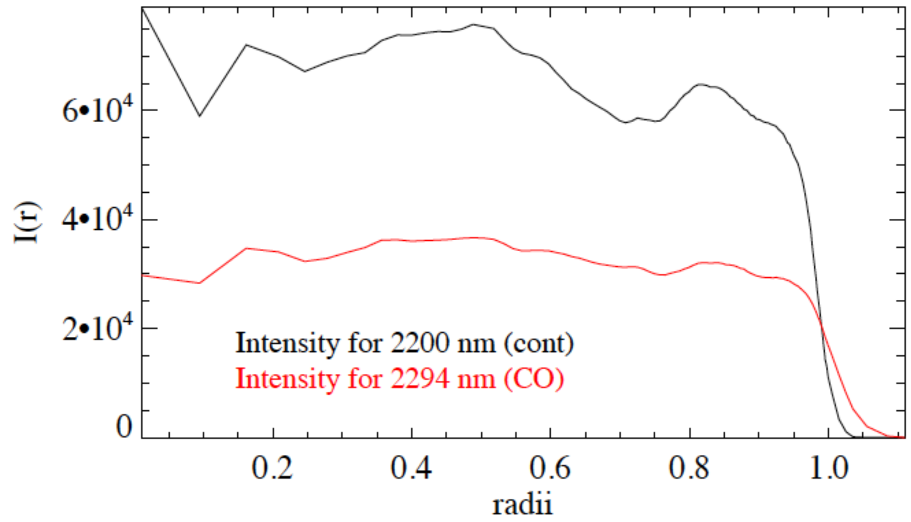

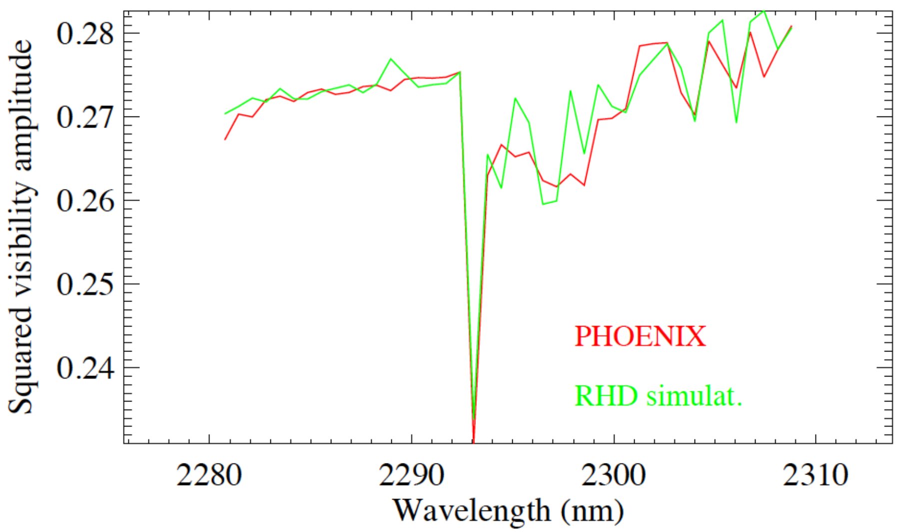

- The intensity in the CO line is lower by a factor of about 2 compared to the intensity in the continuum, which is consistent with observed flux spectra
- The CO line surface is slightly more extended than the continuum surface, but only by a few percent (~7% at the limb)
- The model-predicted visibility curves of the 3D RHD simulation are very similar to the hydrostatic PHOENIX model at the AMBER resolution and can thus not explain the large observed atmospheric extensions of RSG stars

Arroyo-Torres et al., 2015

Comparison to pulsation models (V602 Car)

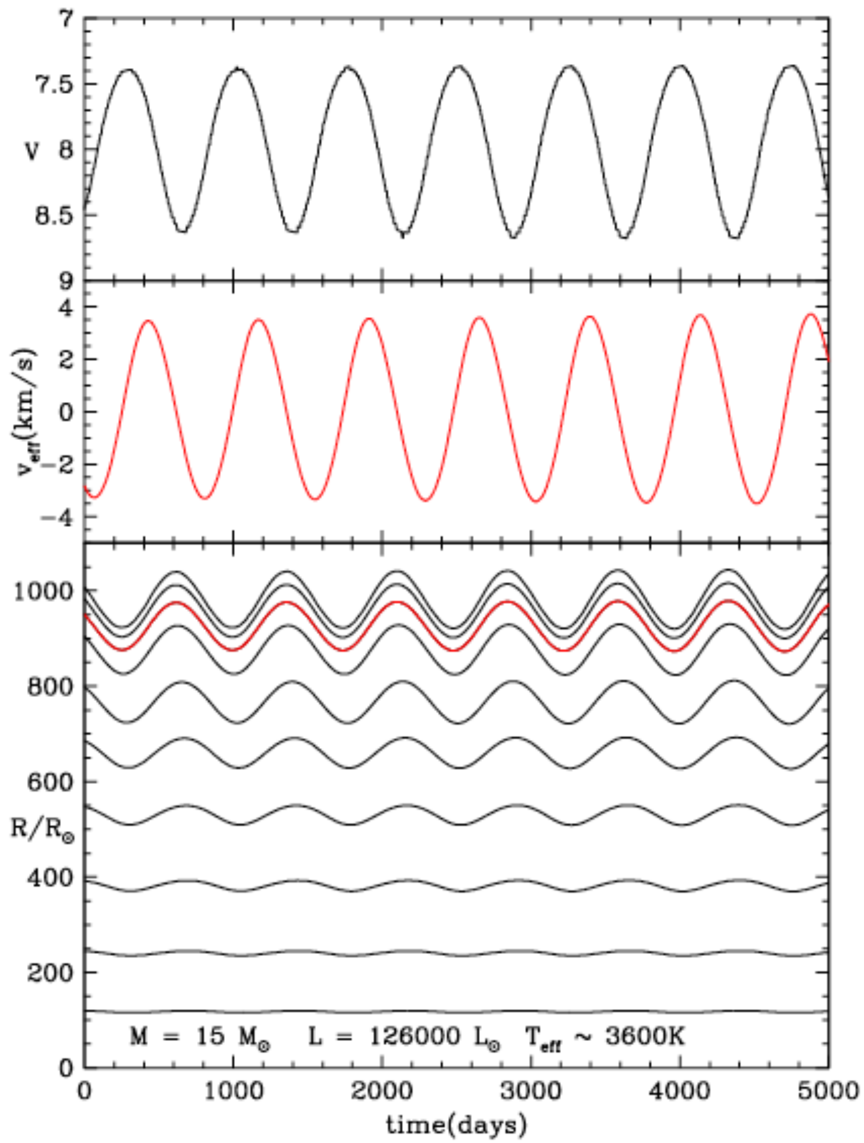

- Amplitude of the photospheric radius variation is about 10% with radial velocities of up to about 5 km/ sec.
- The model reproduces the amplitude of the visual lightcurve of V602 Car of ~ 1 mag
- The velocities are consistent with observed long-term measurements (e.g Gray et al 2008)
- Whilst shock fronts enter the stellar atmosphere in a typical CODEX model of a Mira variable at or below optical depth 1, leading to a geometric extension of the stellar atmosphere of the order a few Rosseland radii it turns out that no shock fronts reach at any phase the atmospheric layers in case of the RSG model.
- The RSG pulsation model leads to an atmosphere as compact as the hydrostatic PHOENIX model, and can not explain the observed atmospheric extensions

Arroyo-Torres et al., 2015

Alternative mechanisms for RSGs

- Velocities higher than those predicted by pulsation models have been observed on time scales much shorter than the variability period (e.g. Josselin & Plez 2007, Gray et al. 2008) . Possibly caused by convective motion.
- There is an observed correlation of atmospheric extension with increasing luminosity, pointing to a radiatively driven acceleration
- Hypothesis: Higher velocities and shocks give rise to a significant Doppler shift, so that radiation pressure on Doppler-shifted lines could accelerate the material -- in a way reminiscent of what happens in the winds of hot stars
- Dust might form at small radii (a few stellar radii) as for Miras and acceleration on dust grains might drive the wind

Arroyo-Torres et al., 2015

RSGs in the HR diagram

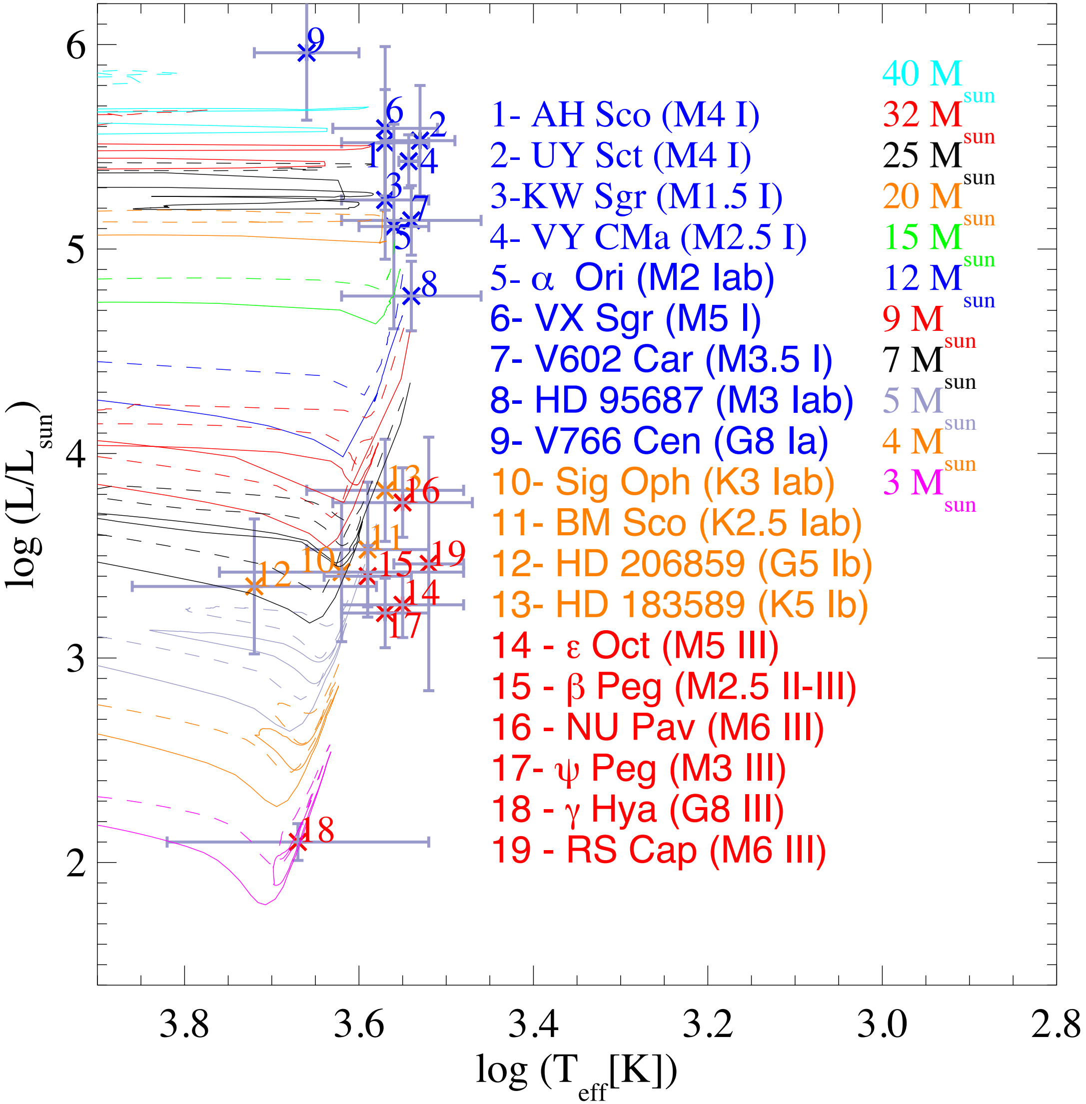

Arroyo-Torres et al., in prep

VLTI/PIONIER images of the RSG VY CMa and the Mira star R Car

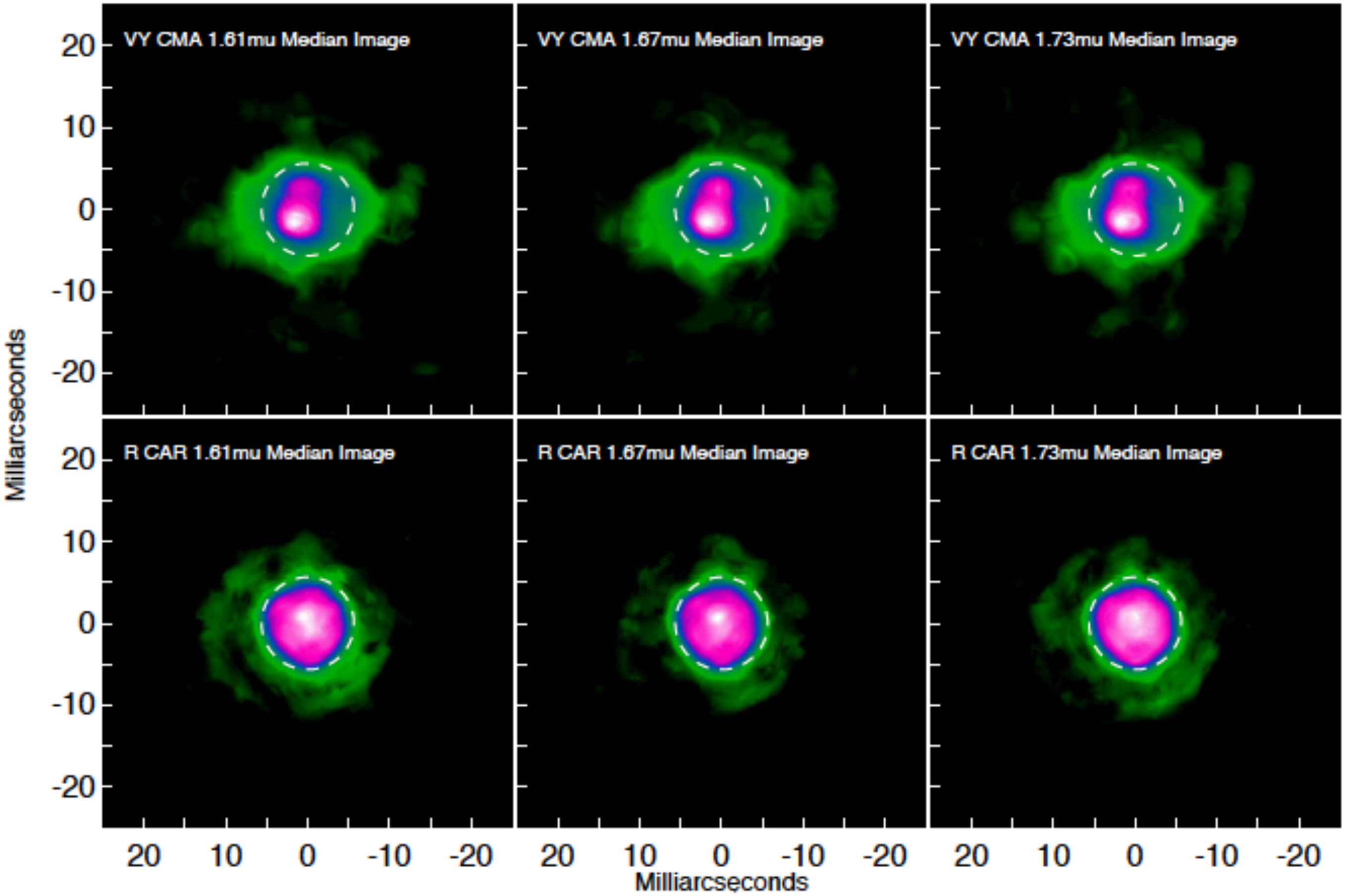

Monnier et al. 2014, SPIE, 9146, 91461Q

Summary: Molecular layers

- 1D dynamic model atmospheres based on self-excited pulsation models, as well as 3D simulations including convection and pulsation are consistent for the overall atmospheric structure and can both explain observed atmospheric extensions of Miras
- Shocks induced by convection and pulsation in 3D models are roughly spherically expanding and of similar nature as shock in 1D pulsation models
- However, neither 1D nor 3D models can explain observed extensions of red supergiants, indicating a missing mechanism
- Observed correlation of atmospheric extension with luminosity for RSGs supports a scenario of radiative acceleration on molecular lines
- First near-IR images obtained with interferometry show dominant (mass-loosing) spots, which is relevant for the mass-loss process

VLTI/MDI OBSERVATIONS OF AGB STARS: DUST FORMATION

Seed particles and dust condensation

- Titanium and aluminum oxides: Dust formation starts with TiO clusters, which can serve as growth centers for both Al_2O_3 and silicates (Gail & Sedlmayer 1999). Al_2O_3 can also condense on its own with condensation temperatures around 1400 K. Al_2O_3 grains may become coated with silicates at larger radii and can serve as seed nuclei for the subsequent silicate formation (e.g. Deguchi 1980, and others).

- Heteromolecular condensation of iron-free magnesium-rich (forsterite) silicates based on Mg, SiO, H_2O (Goumans & Bromley 2012). Such grains may exist at small radii (1.5 ..2 R_*) (Ireland et al. 2005, Norris et al. 2012). Micron-sized grains may drive the wind (Höfner 2008). However, Sacuto et al. (2013) needed to add Al_2O_3 grains to explain interferometric data.

- SiO cluster formation as seeds for silicate dust formation. Thought to take place at temperatures below 600 K; New measurements indicate higher SiO condensation temperatures, and may be compatible with dust temperatures around 1000 K (Gail et al. 2013).

MIDI observations of S Ori: Al_2O_3 grains

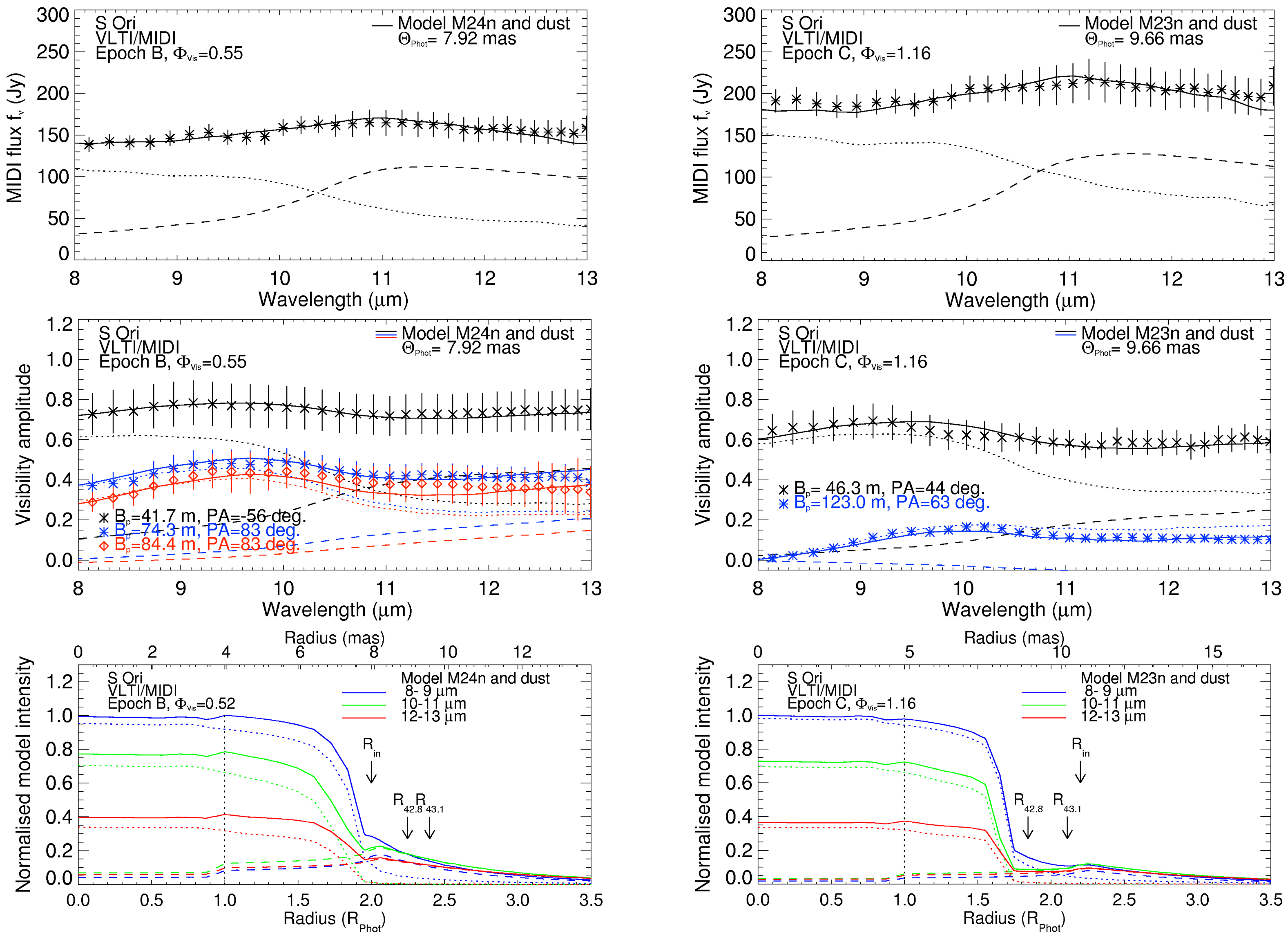

Total flux

Visibility

Model intensity

Wittkowski et al. 2007

MIDI observations of RR Aql: Silicates

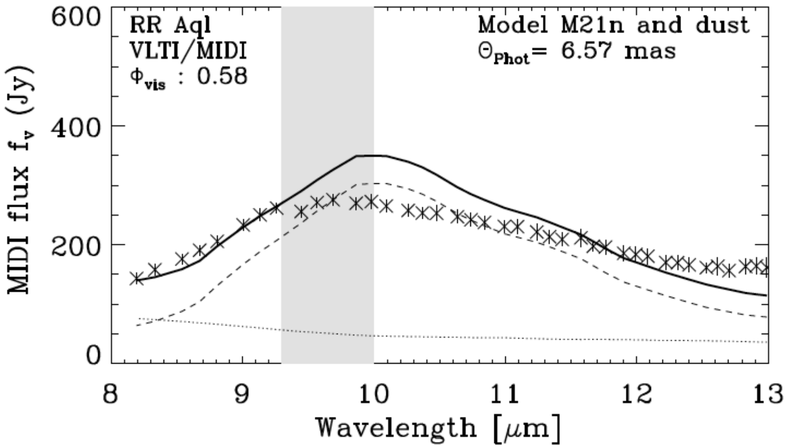

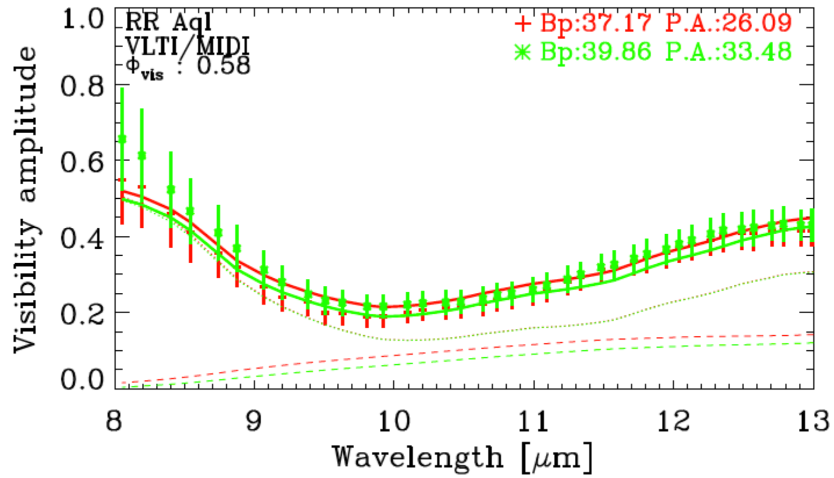

Model	τ_V (Al_2O_3)	τ_V (silicate)	R_{in}/R_{Phot} (silicate)	p (silicate)	Θ_{Phot} [mas]
M21n	0.0	2.8 ± 0.8	4.1 ± 0.7	2.6 ± 0.3	7.6 ± 0.6

- Modeling approach of a silicate dust shell is well consistent with our data.
- No detection of intra-cycle and cycle-to-cycle variability of the dust shell within our uncertainties; consistent with our modeling approach
- MIDI data are not sensitive to an additional Al_2O_3 dust shell with relatively low optical depth.

Karovicova et al. 2011

Dust condensation sequence

- Additional targets (S Ori, R Cnc, GX Mon) processed in the same way:
- Al_2O_3 dust confirmed with an inner radius of ~ 2 photospheric radii; silicate dust with an inner radius of ~4 photospheric radii.
- No evidence of intra-cycle and cycle-to-cycle variations.
- Modeled dust temperatures at the inner radii are consistent with dust condensation temperatures of Al_2O_3 (~1400 K) and warm silicates (~1000 K)

		Mass-loss rate	τ_V	R_{in}/R_{Phot}
R Cnc	Al_2O_3 dust	$0.2\ 10^{-7}\ M_{sun}/yr$	1.4	2.2
S Ori	Al_2O_3 dust	2.2	1.5	1.9
RR Aql	Silicate dust	9.1	2.8	4.1
GX Mon	Al_2O_3 + Silicate dust	54	1.9 / 3.2	2.1 / 4.6

- Dust content of stars with low mass-loss rates dominated by Al_2O_3, while dust content of stars with higher mass-loss rates predominantly exhibit significant amount of silicates, as suggested by Little-Marenin & Little (1990), Blommert et al. (2006).

Karovicova et al. 2013

Aluminum number densities

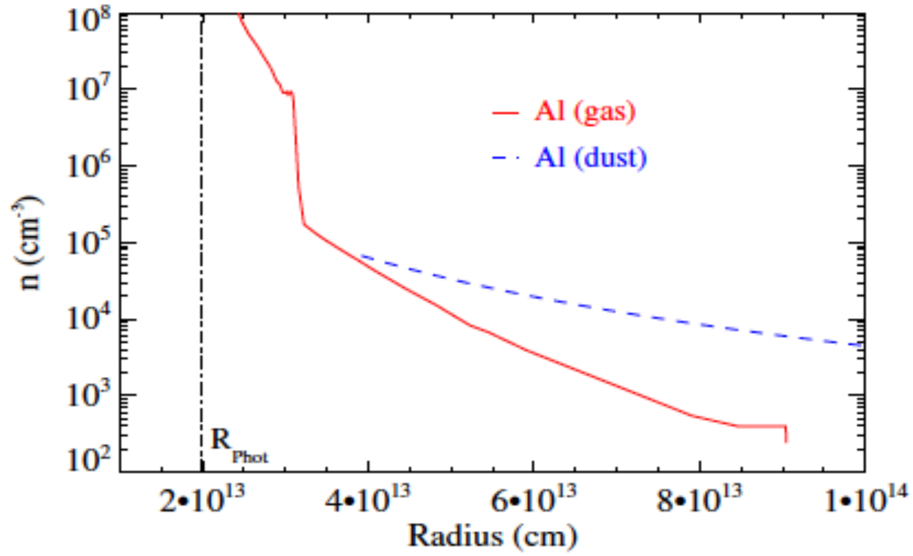

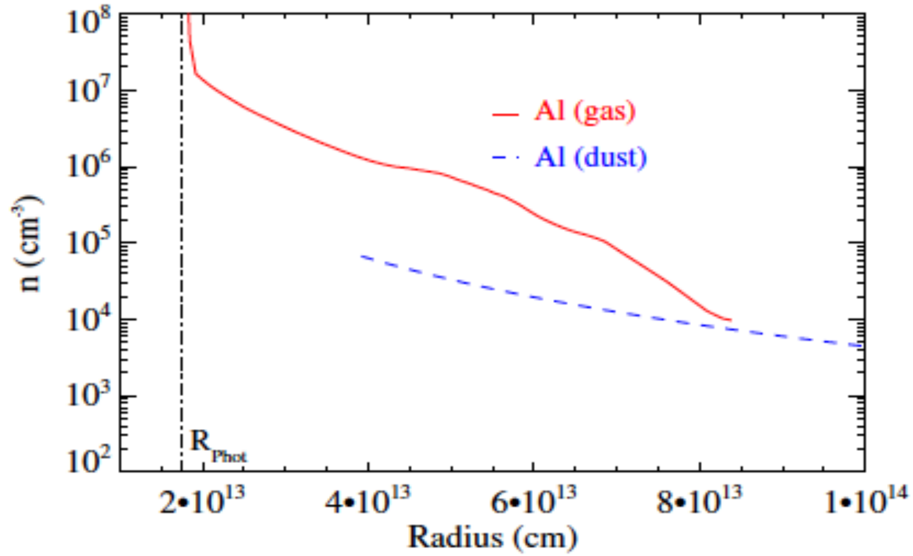

- Overall, the aluminum number densities are not consistent with a dust shell model that consists only of Al_2O_3
- In a sufficiently extended atmosphere, the number density of aluminum can match that of the best-fit dust shell near the inner radius, up to the condensation radius of warm silicates
- Al_2O_3 can be seed particles for the further dust formation

Karovicova et al. 2013

Our Hypothesis (Seeds):

- While Al_2O_3 grains may not be important for the wind driving mechanism, they can be important seed particles for the further dust formation:
  - Small observed dust radii corresponding to 1200K-1300K, consistent with Al_2O_3 condensation temperature; small dust radii consistent with Norris et al. (2012)
  - Good agreement between MIDI data and Al_2O_3 model, in particular regarding the broad feature at 9-13 mu that is attributed to amorphous Al_2O_3
  - Aluminum number densities consistent up to ~4 R_* or ~2 R_{in}

Karovicova et al. 2013

Our Hypothesis (Condensation sequence):

- Sources modeled with Al_2O_3 only:
  - Number densities of Al sufficient to form Al_2O_3 grains in numbers consistent with our radiative transfer models up to ~4 R_* or ~2 R_{in}
  - Serve as seed particles for dust grains that preserve the spectral properties of Al_2O_3 (iron-free silicates, metallic iron, FeO, MgO)
  - Dust formation freezes out at this point
- Sources modeled with Al2O3 and warm silicates:
  - Associated with larger dust optical depths and higher mass-loss rates
  - Dust condensation sequence continues to form amorphous silicates such as olivine or pyroxene
- Sources modeled with warm silicates only:
  - As above, but Al_2O_3 obscured
  - Or different process, such as SiO nucleation or hetermolecular silicate formation at larger radii without Al_2O_3 seeds

Karovicova et al. 2013

Models by Gobrecht, Cherchneff et al. (2015)

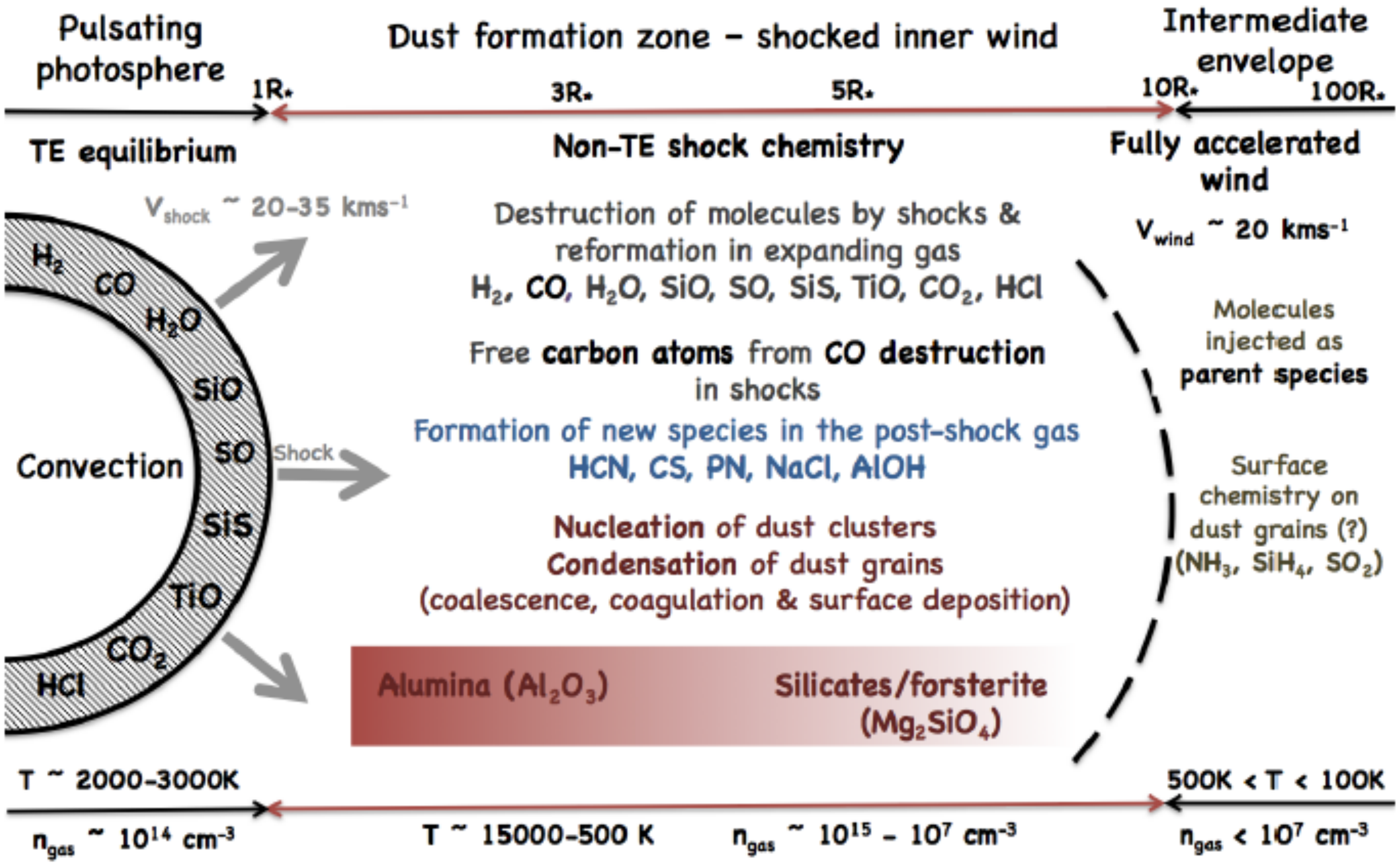

Fig. 1. A schematic view of the dust formation zone in O-rich AGB stars, which includes typical physical parameters and the prevalent chemical processes related to dust production. Molecules present under TE in the photosphere are shown.

Models by Bladh, Höfner et al. (2015)

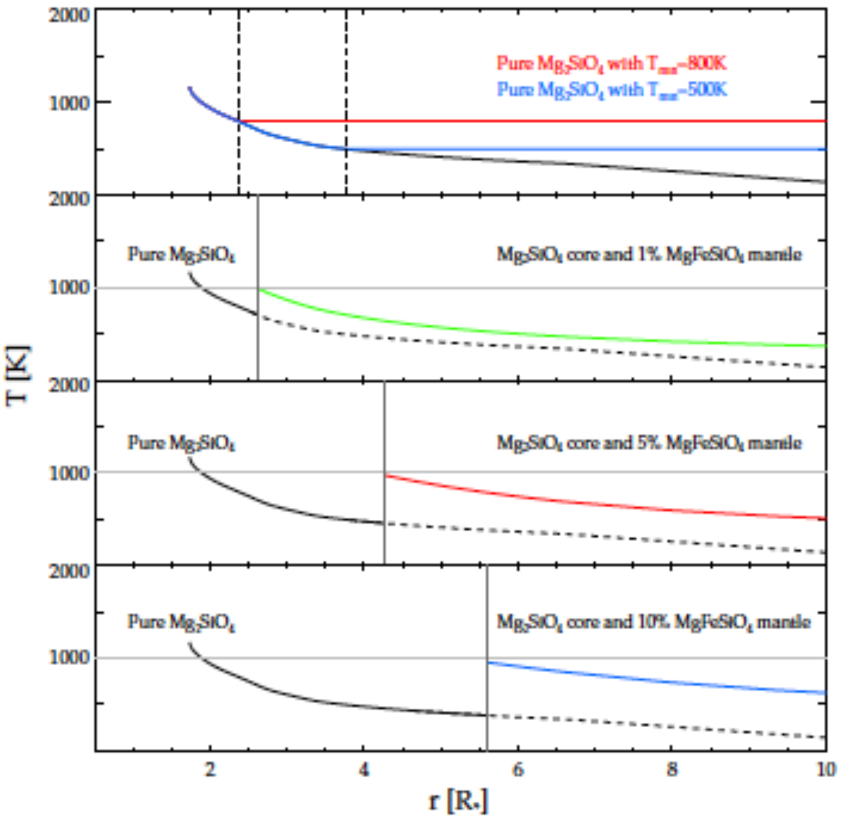

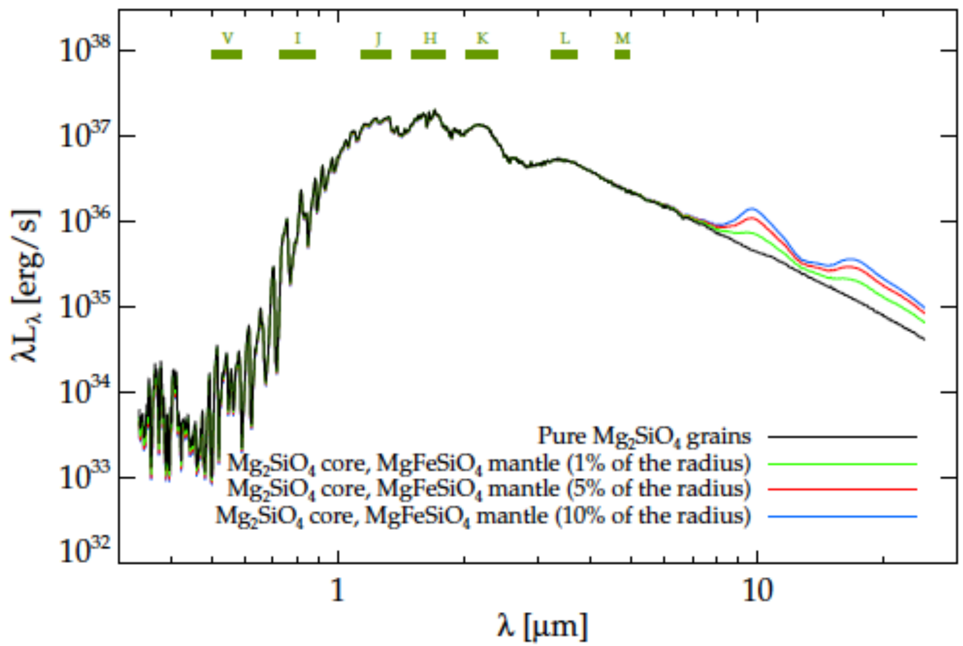

Summary: Dust

- MIDI observations of oxygen-rich Mira stars are consistent with Al_2O_3 dust shells with inner radii of about 2 stellar radii and silicate dust shells with inner radii of about 4 stellar radii. Dust temperatures are consistent with condensation radii of these grains.
- Number densities of aluminum can be large enough in sufficiently extended atmospheres to match the number densities of Al in Al_2O_3 shells. Al_2O_3 grains can thus be seed particles for the further dust condensation.
- Stars with low mass-loss rates predominantly form dust that preserves the spectral properties of Al_2O_3. Stars with higher mass-loss rates form dust with properties of warm silicates.
- Way forward: Direct comparison to self-consistent models

Spectro-
Interferometry

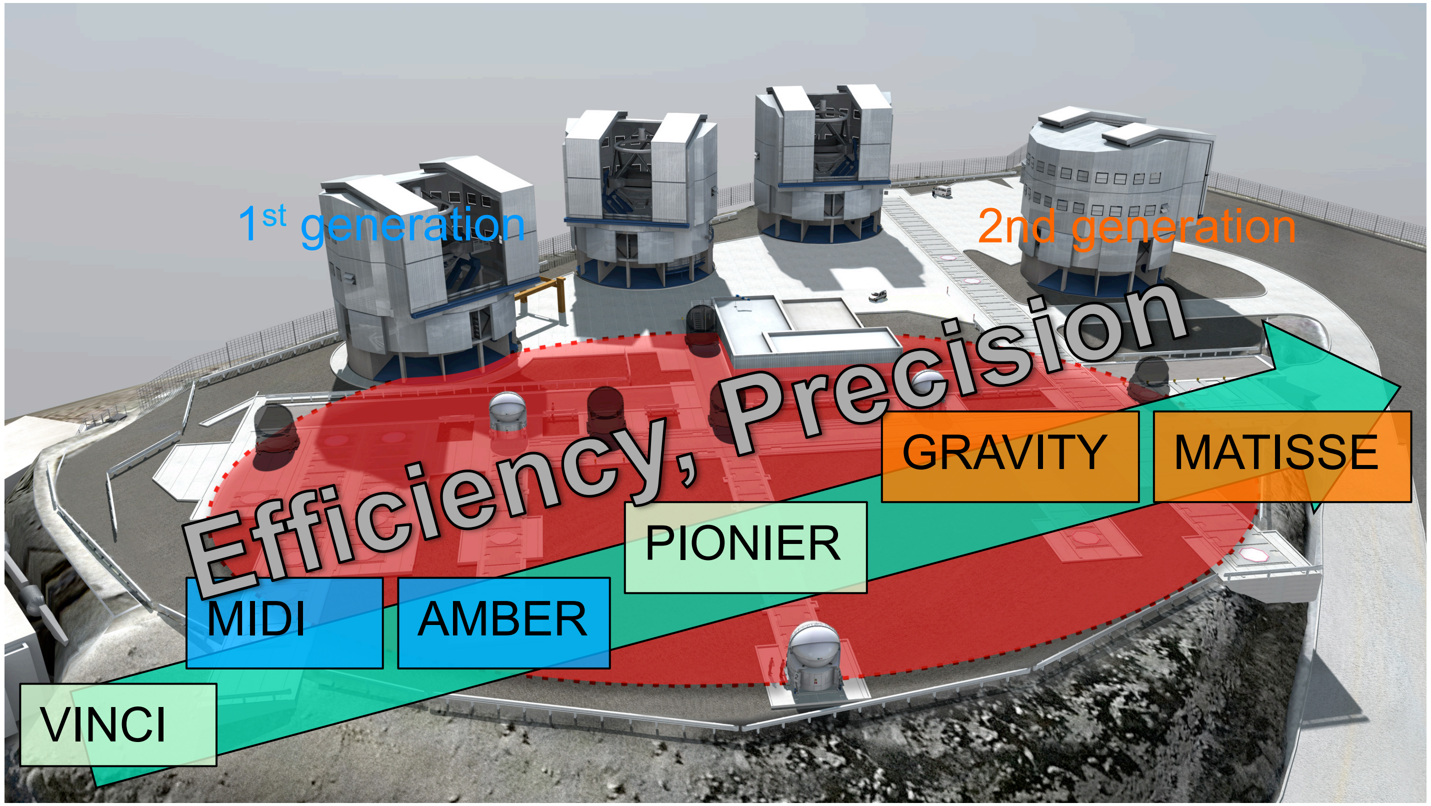

Spectro-
Imaging

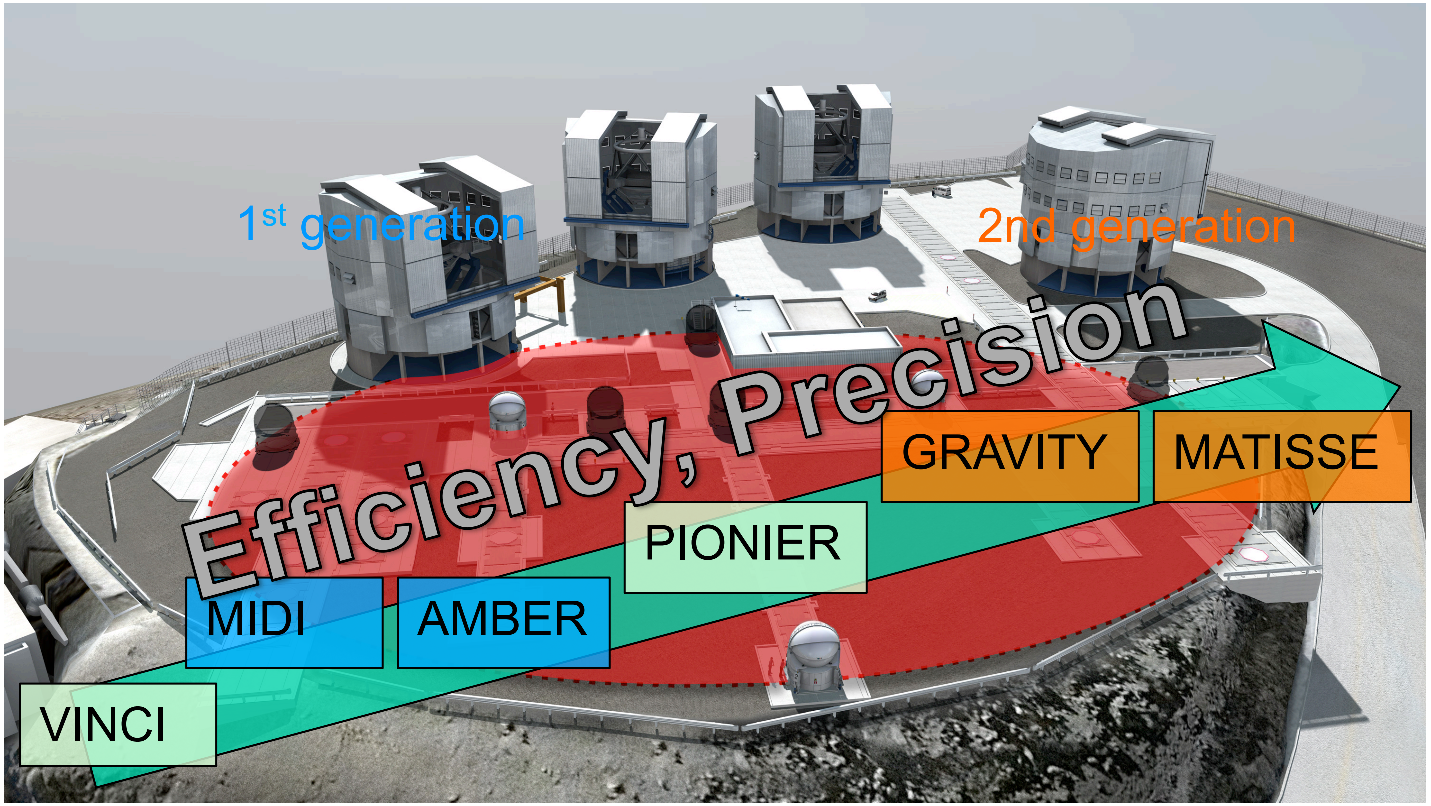

Spectro-Imaging

Monitoring

Spectro-Interferometry

Snapshots

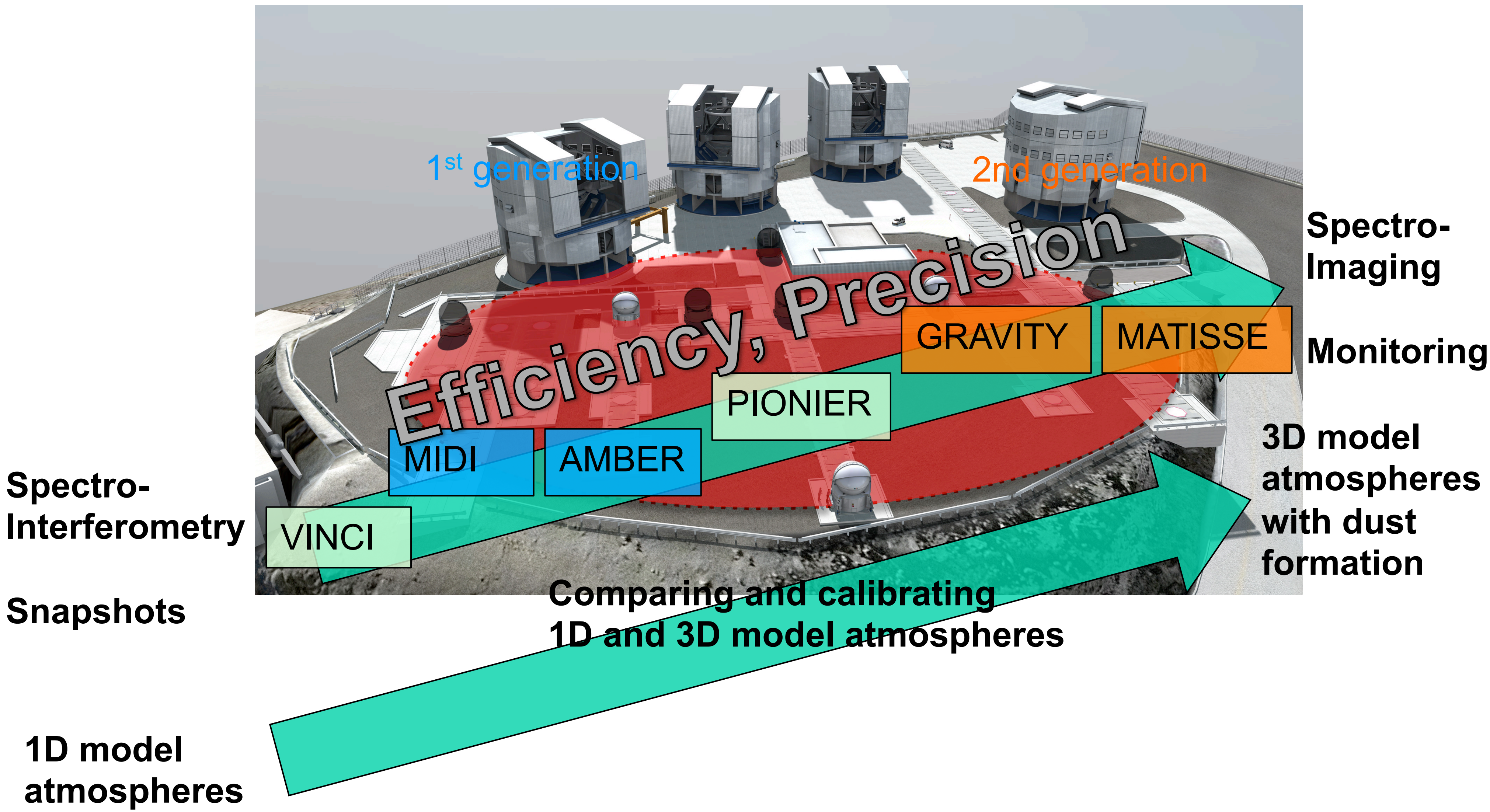
1st generation
2nd generation
Efficiency, Precision
Spectro-
Imaging
GRAVITY
MATISSE
Monitoring
PIONIER
MIDI
AMBER
3D model
atmospheres
with dust
formation
Spectro-
Interferometry
VINCI
Snapshots
Comparing and calibrating
1D and 3D model atmospheres
1D model
atmospheres

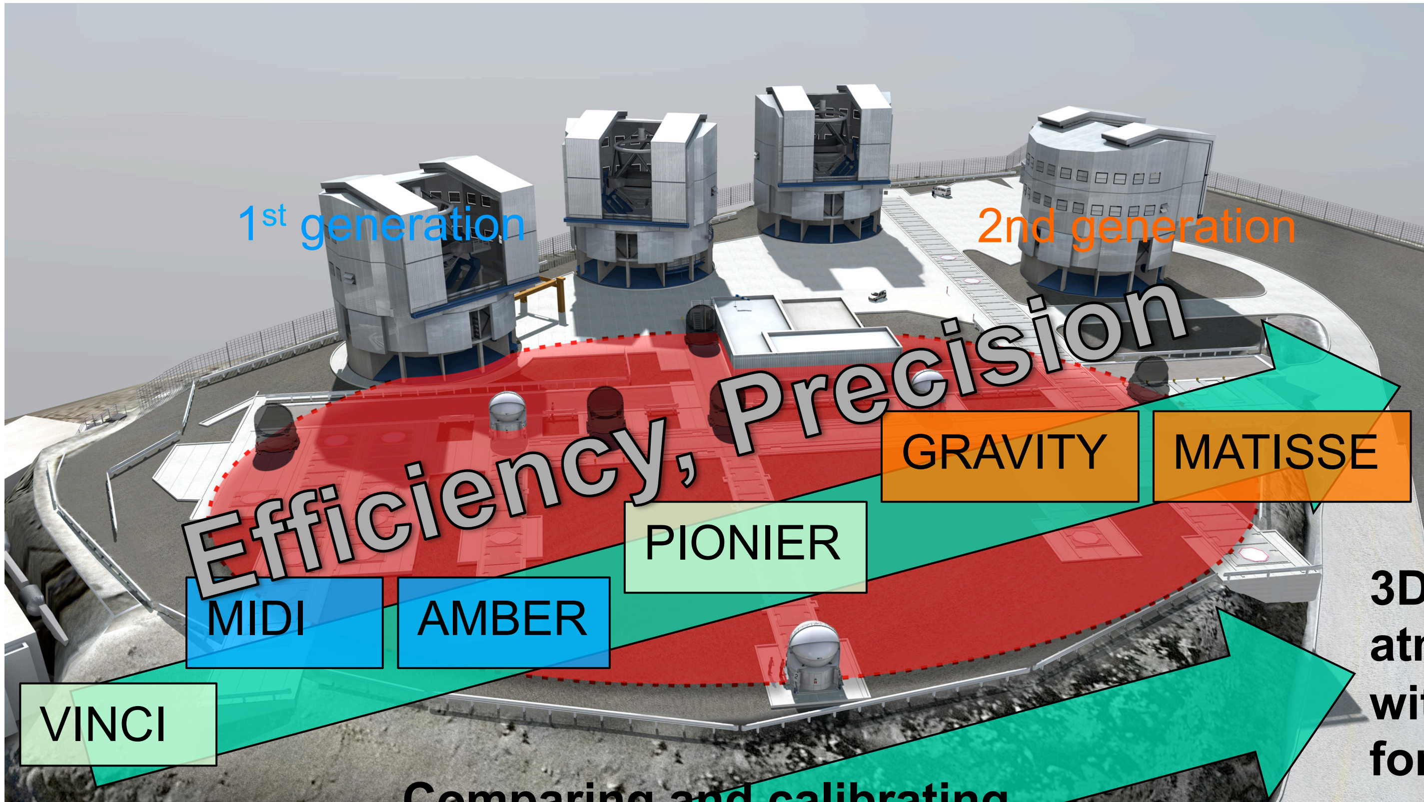

Spectro-Interferometry

Snapshots

1D model atmospheres

Mostly Miras

Comparing and calibrating 1D and 3D model atmospheres

Spectro-Imaging

Monitoring

3D model atmospheres with dust formation

Consolidated understanding of mass loss from all types of cool evolved stars including RSGs

Synergy with ALMA sub-mm interferometry

Synergy with AO / high-resolution spectroscopy